NACA

RESEARCH MEMORANDUM

AERODYNAMIC CHARACTERISTICS OF FOUR WINGS

OF SWEEPBACK ANGLES 0°, 35°, 45°, AND 60°, NACA 65A006

AIRFOIL SECTION, ASPECT RATIO 4, AND TAPER RATIO 0.6 IN

COMBINATION WITH A FUSELAGE AT HIGH SUBSONIC MACH

NUMBERS AND AT A MACH NUMBER OF 1.2

By Arvo A. Luoma

Langley Aeronautical Laboratory
Langley Field, Va.

NATIONAL ADVISORY COMMITTEE
FOR AERONAUTICS

WASHINGTON
June 6, 1951

NATIONAL ADVISORY COMMITTEE FOR AERONAUTICS

RESEARCH MEMORANDUM

AERODYNAMIC CHARACTERISTICS OF FOUR WINGS

OF SWEEPBACK ANGLES 0°, 35°, 45°, AND 60°, NACA 65A006

AIRFOIL SECTION, ASPECT RATIO 4, AND TAPER RATIO 0.6 IN

COMBINATION WITH A FUSELAGE AT HIGH SUBSONIC MACH

NUMBERS AND AT A MACH NUMBER OF 1.2

By Arvo A. Luoma

SUMMARY

An investigation was made in the Langley 8-foot high-speed tunnel of the effect of sweepback angle on wing-fuselage characteristics at subsonic Mach numbers up to approximately 0.95 and at one supersonic Mach number of 1.2. Sweepback angles of 0°, 35°, 45°, and 60° based on the 25-percent-chord line were investigated. Lift, drag, and pitching-moment coefficients were determined from strain-gage measurements. Downwash-angle and total-pressure measurements were made in the region of a probable tail location. The Reynolds number of the tests based on the mean aerodynamic chord varied with Mach number and at the maximum subsonic Mach number was 2×10^6.

Adverse compressibility effects on lift, drag, pitching moment, and maximum lift-drag ratio were reduced by an increase in sweepback angle. The maximum lift-drag ratio at Mach numbers from approximately 0.88 to 0.95 increased with an increase in sweepback angle up to 45° and then decreased between sweep angles of 45° and 60°. At a Mach number of 1.2, the maximum lift-drag ratio increased with an increase in sweepback angle up to the maximum sweep angle of 60°. Abrupt, unstable changes in pitching-moment coefficient, attributed to wing-tip stalling, occurred with an increase in lift coefficient for sweepback angles of 35°, 45°, and 60° at subsonic Mach numbers. An increase in sweepback angle increased the severity of the unstable changes and reduced the lift coefficient at which these changes began.

INTRODUCTION

A phase of the general program on transonic research being con-
ducted by the National Advisory Committee for Aeronautics includes tests
of wing-fuselage configurations with systematic variations of the vari-
ous wing geometric parameters including sweep angle, aspect ratio, taper
ratio, and thickness ratio. Several of the research facilities at the
Langley Aeronautical Laboratory have been used for these tests. The low-
speed aerodynamic characteristics of several of the wings through a
range of Reynolds numbers have been obtained in the Langley two-
dimensional low-turbulence pressure tunnel. Data throughout the trans-
onic speed range have been obtained for most of the configurations
included in the transonic-wing program from tests on the transonic bump
in the Langley high-speed 7- by 10-foot tunnel. Rocket-powered flight
tests of some of the configurations have been made and such tests pro-
vided zero-lift drags throughout the transonic speed range at high
Reynolds numbers. Further tests of several of the configurations have
been made at the Ames Aeronautical Laboratory.

A recent investigation of the sweep series in the Langley 8-foot
high-speed tunnel provides information up to high-subsonic Mach numbers
and for one supersonic Mach number of 1.2. These data have been pub-
lished in basic form in references 1 to 4. A comparison of the charac-
teristics of the sweep series as affected by different testing techniques
is given in reference 5.

The purpose of the present paper is to analyze and summarize the
information on the effects of sweep on wing-fuselage characteristics
obtained in the investigation of the sweep series in the Langley 8-foot
high-speed tunnel. Sweepback angles of 0°, 35°, 45°, and 60° were
included in the tests. Lift, drag, pitching moment, downwash angles
and total-pressure losses in the vicinity of a probable tail location,
and the static pressure at the base of the fuselage were measured.

SYMBOLS

The aerodynamic coefficients and other symbols used in this paper
are defined as follows:

A   aspect ratio of wing $\left(b^2/S\right)$

a   speed of sound in undisturbed stream

b   span of wing

C_D drag coefficient $\left(\dfrac{D}{qS}\right)$

C_L lift coefficient $\left(\dfrac{L}{qS}\right)$

C_m pitching-moment coefficient about lateral axis which passes through 25-percent point of mean aerodynamic chord of wing

$\left(\dfrac{M_{c'/4}}{qc'S}\right)$

c section chord of wing, measured parallel to plane of symmetry of model

c' mean aerodynamic chord of wing $\left(\dfrac{2c_r}{3}\dfrac{1 + \lambda + \lambda^2}{1 + \lambda}\right)$

c_t nominal tip chord of wing, obtained by extending leading and trailing edges of wing to plane parallel to plane of symmetry of model and passing through wing tip

c_r root chord of wing, obtained by extending leading and trailing edges of wing to plane of symmetry of model

D drag

H total pressure of undisturbed stream

H_t total pressure of stream at rake position

ΔH loss in total pressure $(H - H_t)$

L lift

M Mach number $\left(\dfrac{V}{a}\right)$

$M_{c'/4}$ pitching moment of aerodynamic forces about lateral axis which passes through 25-percent point of mean aerodynamic chord of wing

P_b base-pressure coefficient $\left(\dfrac{p_b - p}{q}\right)$

p static pressure in undisturbed stream

p_b static pressure on surface of sting at base of fuselage (fig. 4)

q dynamic pressure in undisturbed stream $\left(\frac{1}{2}\rho V^2\right)$

R Reynolds number $\left(\frac{\rho V c'}{\mu}\right)$

S area of wing $\left(b\frac{c_r + c_t}{2}\right)$

V velocity in undisturbed stream

α angle of attack of model, based on fuselage reference axis

ϵ "point" downwash angle as determined from yaw-tube measurements

Λ angle of sweep of wing, based on 25-percent-chord line

λ taper ratio of wing $\left(\frac{c_t}{c_r}\right)$

μ coefficient of viscosity in undisturbed stream

ρ mass density in undisturbed stream

Subscripts:

max   maximum value

APPARATUS AND METHODS

Tunnel and Model Support

The tests were made in the Langley 8-foot high-speed tunnel which, for these tests, was of the closed-throat type with the subsonic and supersonic test sections of circular cross section. The Mach number distribution was uniform in the subsonic test section and was within ±0.02 of the design Mach number of 1.2 in the supersonic test section (reference 6). The models were supported on a sting (fig. 1), which is capable of being moved longitudinally along the tunnel axis for testing in either the subsonic test section or the supersonic test section (fig. 2). A more detailed discussion of the sting support apparatus is given in reference 1.

Models and Balance System

Four wings of different sweep angles were tested on a common fuselage without tail surfaces. The wings were mounted on the fuselage in the midwing position at zero incidence and with the 25-percent point of the mean aerodynamic chord located at the maximum-diameter station of the fuselage. All the wings had NACA 65A006 airfoil sections parallel to the model plane of symmetry, an area of 1 square foot, an aspect ratio of 4, and a taper ratio of 0.6. Sweep angle was the only geometric parameter which was varied. Sweepback angles of 0°, 35°, 45°, and 60° based on the 25-percent-chord line were investigated. The ordinates for the NACA 65A006 airfoil section, together with the ordinates for the fuselage, are given in table 1, and the dimensions of the models are given in figure 3. The wings with sweepback angles of 0°, 45°, and 60° were made of aluminum alloy. The wing with a sweepback angle of 35° consisted of a steel core covered with a skin of bismuth-tin alloy.

The shape of the fuselage used in the present tests was a body of revolution of fineness ratio 10, achieved by the cutting-off of the rear one-sixth of a basic fuselage shape of fineness ratio 12 (table I). The maximum diameter was located at 50 percent of the basic fuselage length. The base diameter of the test fuselage was one-half the maximum diameter. The test fuselage was made of steel.

A strain-gage balance was housed within the fuselage, and attachment between the balance and the fuselage was made at the forward portions of the fuselage and balance. The rear portion of the balance faired into the sting.

Test Procedure

Lift, drag, and pitching-moment coefficients were determined from strain-gage measurements, and point downwash angles and wake surveys in the region of a probable tail location were obtained from yaw-tube and total-pressure measurements. The test data for the fuselage alone are presented in reference 1 and for the wing-fuselage configurations in references 1 to 4.

Two combination yaw-tube and total-pressure rakes were used in making the downwash and wake surveys (fig. 4). The rakes were located 1.225 wing semispans behind the 25-percent point of the wing mean aerodynamic chord and the planes of the rakes were parallel to the model plane of symmetry and located 0.083 and 0.292 wing semispan from the model plane of symmetry. The three yaw tubes in each rake were located 0.125, 0.250, and 0.375 wing semispan above the chord plane of the wing; the seven total-pressure tubes in each rake were located as shown in figure 4.

The static pressure on the surface of the sting at the base of the fuselage was measured for all test conditions. The orifice location is indicated in figure 4.

Data were obtained at subsonic Mach numbers from 0.6 to approximately 0.95 and at one supersonic Mach number of 1.2. An optical method was used for determining the angle of attack of the model and this method is described in reference 1. The angle-of-attack range extended from -2° up to the angle of attack which, for most cases, approximately corresponded to the maximum allowable load of either the strain-gage balance or the wing. The variation of test Reynolds number (based on a mean aerodynamic chord of 6.125 inches which was the same for all wings) with test Mach number is given in figure 5.

CORRECTIONS AND PRECISION

Tunnel-wall-interference corrections have been applied to the data (references 1 to 4) by the methods discussed in reference 1. The corrections to the Mach number reached a maximum of approximately 1.5 percent at a Mach number of 0.96.

Sting interference.- The present tests did not include the determination of the interference effect of the sting on the measured aerodynamic forces, moments, base pressures, and downwash angles.

Sting-interference data at low angles of attack are available from the tests of reference 7 on a comparable wing-fuselage configuration and sting support. On the basis of the tests of reference 7, it is indicated that, for the fuselage alone and the wing-fuselage configuration of the present tests, the effect of sting interference at low angles of attack would be negligible on lift coefficient and pitching-moment coefficient, would require the addition to the measured drag coefficients of a drag-coefficient increment of approximately 0.003 at subsonic Mach numbers and approximately 0.002 at a Mach number of 1.2, and would require the addition to the measured base-pressure coefficients of a base-pressure-coefficient increment of approximately -0.1 at all test Mach numbers.

In the tests of reference 7 point downwash angles were not obtained, but an effective downwash angle in the region of the horizontal tail was determined from measurements of the lift and pitching moment of the configurations consisting of complete model and complete model less horizontal tail. The sting-interference corrections to the effective downwash angle in the tests of reference 7 required the addition to the uncorrected values of an effective-downwash-angle increment of the order

of 1° at subsonic Mach numbers and 0.2° at a Mach number of 1.2. On the basis of this information the sting-interference corrections to the measured point downwash angles of the present tests would be expected to be large at subsonic Mach numbers and probably small at a Mach number of 1.2. The magnitude of the sting-interference corrections would also be expected to be different at the two spanwise rake stations and, perhaps, at the individual yaw tubes at a given rake station.

No sting-interference corrections have been made to the data of the present tests except in the determination of maximum lift-drag ratios since the sting-interference data of reference 7 strictly apply only for the specific configurations investigated in the tests of reference 7 and were obtained only at low angles of attack. Additional discussion on sting interference is given in reference 1.

Aeroelasticity.- The bending of a swept wing under aerodynamic load results in a change in the spanwise variation of the local angle of attack measured parallel to the plane of symmetry of the airplane and, consequently, in a modification of the span loading. An estimation of the bending of the sweptback wings of the present tests under aerodynamic load and the resultant effect on lift and pitching-moment coefficients was made in the analyses of references 1, 2, and 4 for one Mach number, using theoretical basic and additional span loadings from references 8 and 9 and flexural rigidity characteristics determined from static bending tests. The calculations indicated that the aeroelastic bending effects for the sweptback wings were appreciable, resulting in a decrease in lift-curve slope and a forward movement of the aerodynamic center. As an example, the calculations for the configuration with 45° of sweepback indicated that, at a Mach number of 0.80, wing bending under aerodynamic load resulted in a reduction in the lift-curve slope of approximately 7 percent and a forward movement of the aerodynamic center of approximately 2 percent of the mean aerodynamic chord. An increase in sweepback angle increased the aeroelastic effects on lift-curve slope and movement of the aerodynamic center.

No corrections have been made to the data presented herein for aeroelastic wing bending.

Precision.- An estimation of the accuracy of the strain-gage measurements, made in the analysis of reference 1, indicated that the measured values of lift, drag, and pitching-moment coefficients (including the effect of sting interference) were within approximately ±0.01, ±0.001, and ±0.005, respectively, throughout the Mach number range.

The angle of attack α was estimated to be accurate within ±0.1°.

RESULTS

The present paper is mainly concerned with the effects of sweepback angle on the characteristics of the wing-fuselage configuration. Data for the various sweptback configurations are given on the same figures, and these figures, for the most part, show the variation of the aerodynamic parameters with Mach number. Data for the fuselage alone are also included in a few of the figures. In several of the figures only representative test Mach numbers and angles of attack are included; the complete test data are given in references 1 to 4.

The variation of lift coefficient with Mach number at constant values of angle of attack and the variation of lift coefficient with angle of attack for several values of Mach number are shown in figures 6 and 7, respectively. Figure 8 presents the variation of lift-curve slope with Mach number at two values of lift coefficient.

The variation of drag coefficient with Mach number is shown in figure 9 at constant values of angle of attack, and in figure 10 at constant values of lift coefficient. Figure 11 presents the variation of drag coefficient with lift coefficient at several Mach numbers.

The variation of maximum lift-drag ratio with Mach number is shown in figure 12, and the lift coefficient for maximum lift-drag ratio plotted against Mach number is shown in figure 13. A sting-interference correction of 0.003 at subsonic Mach numbers and 0.002 at a Mach number of 1.2 were added to the measured drag coefficients in the determination of maximum lift-drag ratio and the lift coefficient for maximum lift-drag ratio. These corrections were based on the sting-interference data of reference 7.

The variation of pitching-moment coefficient with Mach number is presented in figure 14 at constant values of angle of attack, and in figure 15 at constant values of lift coefficient. The variation of pitching-moment coefficient with lift coefficient is shown in figure 16 for several values of Mach number. Figure 17 presents the variation of the pitching-moment-curve slope parameter $\partial C_m/\partial C_L$ with Mach number at two values of lift coefficient.

The variation of point downwash angle with angle of attack is shown in figure 18. Both rakes used were located 1.225 wing semispans behind the 25-percent point of the wing mean aerodynamic chord. Figure 18(a) presents downwash data for the rake located 0.083 wing semispan from the model plane of symmetry for the three yaw-tube locations and figure 18(b) presents similar data for the rake located 0.292 wing semispan from the

model plane of symmetry. Total-pressure measurements $\Delta H/q$ are shown for the two rake positions in figures 19 and 20.

Figure 21 presents data on the static-pressure coefficient on the surface of the sting at the base of the fuselage (fig. 4 indicates the position of the base-pressure orifice).

DISCUSSION

The specifications for the wing-fuselage configurations tested called for an uncambered wing mounted on the fuselage in the midwing position at zero incidence, so that at an angle of attack of zero the lift and pitching moment should be zero. In the actual tests, however, the lift and pitching moment were somewhat different from zero at an angle of attack of zero (figs. 6(a) and 14(a)); this asymmetry may be explained partly by an unintentional small positive incidence of the wings on the fuselage and, perhaps, by the probable existence of a slight initial upflow of the air in the tunnel.

Lift Characteristics

An increase in sweepback angle moderated the compressibility effects on lift-coefficient characteristics, so that at a sweepback angle of 60° the lift coefficient at a given angle of attack was essentially the same at all test Mach numbers (fig. 6). At a Mach number of 1.2 the lift coefficients at a given angle of attack for the configurations with 0°, 35°, and 45° of sweepback were somewhat greater than the corresponding values of a Mach number of 0.6 (figs. 6(b) and 6(c)).

The variation of lift coefficient with angle of attack was generally nonlinear for all angles of sweepback, especially at the subsonic Mach numbers (fig. 7). The lift-curve slope was higher at intermediate lift coefficients than at lift coefficients in the vicinity of zero lift for all angles of sweepback at the subsonic test Mach numbers, except for the unswept configuration at Mach numbers higher than approximately 0.88 where the larger supercritical losses for the unswept configuration at the intermediate lift coefficients reversed the general trends (figs. 7 and 8).

An increase in lift-curve slope at moderate angles of attack has been observed in several low-speed investigations of highly sweptback wings having small leading-edge radii (references 10, 11, and 12). Pressure-distribution and tuft studies of a 45° sweptback wing with sharp leading and trailing edges (reference 10) and pressure-distribution

studies of triangular wings with double-wedge and NACA 65-006.5 airfoil sections (reference 11) indicated the existence of a separation-vortex-flow pattern whereby at relatively low angles of attack the flow separated from the leading edge and then reattached behind the initial separation point, conjointly with the development within the bubble of separated flow of a separation vortex. The chordwise extent of the vortex region increased with increasing spanwise distance from the plane of symmetry. The separation-vortex-flow pattern results in an effective increase in camber and leads in many cases to an increase in lift-curve slope at the moderate angles of attack.

The tests of reference 12, which included wings similar to those investigated in the present tests, were made through a range of Reynolds numbers from 1.5×10^6 to 12×10^6 and at Mach numbers less than approximately 0.20. Increases in lift-curve slope at moderate angles of attack were observed in those tests for the wings with sweepback angles of 45° and 60° at the low Reynolds numbers. An increase in Reynolds number generally decreased the amount of the changes in lift-curve slope occurring at moderate angles of attack or at least delayed the changes in slope to higher angles of attack.

Leading-edge roughness had small effect on the lift characteristics in the tests of reference 12 for all angles of sweepback. In the present tests a transition strip at 10-percent chord had little effect on the lift characteristics of the wings with 45° and 60° of sweepback (see references 1 and 4) but resulted in a reduction in the amount of the increases in lift-curve slope occurring at moderate angles of attack for the unswept wing. (See reference 3.)

The tests of reference 12 showed no increases in lift-curve slope for the unswept wing in the Reynolds number range from 3×10^6 to 12×10^6, but subsequent unpublished data on this wing at higher Mach numbers showed increases in lift-curve slope similar to those occurring for the unswept wing of the present tests. The increases in lift-curve slope for the unswept wings were apparently a consequence of phenomena which were different from those observed for the highly sweptback wings and appear to be associated with compressibility effects.

Theoretical lift-curve slopes at zero lift are included in figure 8. The incompressible lift-curve slopes were obtained from reference 9 and were modified for the first-order effects of compressibility by an adaptation of the Prandtl-Glauert rule as given in reference 13. The theoretical curves are seen to underestimate the compressibility effects at the higher Mach numbers for sweepback angles up to 45° (fig. 8).

At a Mach number of 1.2 the lift-curve slopes at a lift coefficient of 0.4 as compared to those at zero lift were lower for small angles of sweepback and generally higher for large angles of sweepback (fig. 8).

Drag Characteristics

The drag-rise Mach number was delayed to higher values and the rate of the drag rise was reduced by an increase in sweepback angle (figs. 9 and 10).

The drag coefficient at zero lift, or at an angle of attack of 0°, was affected only to a small extent by an increase in sweepback angle at Mach numbers up to 0.875 and was reduced by an increase in sweepback angle up to 60° at test Mach numbers above 0.875, where the supercritical losses increased as sweep angle was reduced (figs. 9(a) and 10(a)). At a Mach number of 1.2 the zero-lift drag coefficient was approximately halved by a change in sweep angle from 0° to 60° (fig. 10(a)).

At the higher angles of attack, the drag coefficient at a given angle of attack was reduced by an increase in sweepback angle up to 60° at all test Mach numbers (figs. 9(b), 9(c), and 9(d)). On the basis of the same lift coefficient, however, an increase in sweep angle had a variable effect on the drag coefficient, depending on the Mach number and the lift coefficient (figs. 10 and 11).

At a lift coefficient of 0.2 at Mach numbers from 0.60 to 0.875, the drag coefficient was essentially unaffected by an increase in sweep-back angle up to 45° and was increased by a change in sweep angle from 45° to 60° (fig. 10(b)). At a lift coefficient of 0.4 at Mach numbers from 0.60 to 0.81 and at a lift coefficient of 0.6 at Mach numbers from 0.73 to 0.84, the drag coefficient increased with an increase in sweep-back angle up to 60° (figs. 10(c) and 10(d)). The difference in the drag coefficients of the configurations with 60° and 0° of sweepback at these conditions was very large. The increase in drag coefficient resulting from an increase in sweepback angle for constant lift-coefficient conditions was probably a consequence of a loss in leading-edge suction accompanying leading-edge separation together with the decrease in lift-curve slope which occurred when the sweep angle was increased, and was probably aggravated by tip stalling of the more highly sweptback wings.

At Mach numbers from 0.875 to 0.95 at a lift coefficient of 0.2 and at test Mach numbers above approximately 0.85 at lift coefficients of 0.4 and 0.6, the increase in the supercritical losses for the unswept configuration modified the previously noted effect of sweep on drag coefficient to the extent that an increase in sweep angle from 0° first

decreased the drag coefficient and then at higher angles of sweepback
increased the drag coefficient (figs. 10(b), 10(c), and 10(d)). At test
Mach numbers above approximately 0.93 at lift coefficients of 0.4 and
0.6, the drag coefficient was reduced by an increase in sweepback angle
up to 45° and was then increased by a change in sweep angle from 45° to
60° (figs. 10(c) and 10(d)). At a Mach number of 1.2 at a lift coef-
ficient of 0.2, the drag coefficient was reduced by an increase in
sweepback angle up to 60° (fig. 10(b)).

Maximum Lift-Drag Ratio

At the lower subsonic Mach numbers the maximum lift-drag ratio was
approximately the same for the configurations with sweep angles of 0°,
35°, and 45°, and was approximately one-sixth less for the configu-
ration with a sweep angle of 60° (fig. 12). At the higher subsonic Mach
numbers large losses in maximum lift-drag ratio occurred with increase
in Mach number for the configurations with sweep angles of 0°, 35°, and
45°, and these losses were delayed to higher Mach numbers by the increase
in sweepback angle (fig. 12). The configuration with 60° of sweepback
did not experience the large changes in maximum lift-drag ratio which
occurred for the configurations with lower sweep.

At Mach numbers from approximately 0.88 to 0.95, the maximum lift-
drag ratio increased with an increase in sweepback angle up to 45° and
then decreased between sweep angles of 45° and 60°. At a Mach number
of 1.2 the maximum lift-drag ratio increased with an increase in sweep-
back angle up to the maximum sweep angle of 60°.

The effect of compressibility on the lift coefficient corresponding
to the maximum lift-drag ratio became less as the sweep angle was
increased (fig. 13). There was a decrease in the lift coefficient cor-
responding to the maximum lift-drag ratio for the unswept configuration
between Mach numbers of 0.80 and 0.875 (fig. 13), and this decrease was
a result of the incremental drag coefficient due to lift for this con-
figuration which increased with an increase in Mach number at test Mach
numbers above 0.80. At test Mach numbers above 0.875, the zero-lift
drag coefficient for the unswept configuration increased with an increase
in Mach number (fig. 10(a)), and this behavior resulted in a lift coef-
ficient corresponding to the maximum lift-drag ratio for the unswept
configuration which increased with an increase in Mach number as shown
in figure 13. In a similar way the lift coefficient corresponding to
the maximum lift-drag ratio for the other configurations increased with
an increase in Mach number at high subsonic Mach numbers, and between
the highest subsonic test Mach numbers and a Mach number of 1.2 (fig. 13)
as a result of the zero-lift drag coefficient which increased with an
increase in Mach number at these Mach numbers (fig. 10(a)).

Pitching-Moment Characteristics

The pitching-moment coefficients of the wing-fuselage configurations generally changed in a negative direction with an increase of Mach number at the higher speeds for all angles of sweepback (figs. 14 and 15). An increase in sweepback angle generally moderated the extent of the variation of pitching-moment coefficient with Mach number (figs. 14 and 15).

The variation of pitching-moment coefficient with lift coefficient for the wing-fuselage configurations was nonlinear at subsonic Mach numbers for all angles of sweepback (fig. 16). At a Mach number of 1.2 the pitching-moment characteristics for the wing-fuselage configurations were more regular for all angles of sweepback (fig. 16(d)). The low-speed tests of reference 12 showed somewhat similar irregular pitching-moment characteristics for the wing alone. In the present tests, the pitching-moment slope $\partial C_m/\partial \alpha$ for the fuselage alone was 0.006 at low angles of attack and approximately 10 percent less at the highest angles of attack, at all test Mach numbers. (See reference 1.) The nonlinearity of the pitching-moment characteristics of the wing-fuselage configurations may be mainly attributed to the wing characteristics.

The configuration with 60° of sweepback experienced an abrupt increase in pitching-moment coefficient with an increase in lift coefficient greater than approximately 0.3 at the subsonic Mach numbers (fig. 16). This instability is associated with complete separation of the flow over the tip sections of sweptback wings (reference 12). The configuration with 45° of sweepback showed the same type of instability at lift coefficients greater than approximately 0.6 at the subsonic Mach numbers, but the severity of the unstable changes was less than that for the configuration with 60° of sweepback (fig. 16). The configuration with 35° of sweepback also appeared to be characterized by this same type of instability but to a lesser extent and at higher lift coefficients than the configuration with 45° of sweepback. No unstable changes of this type occurred in pitching-moment coefficient for the unswept configuration.

The variation with Mach number of the pitching-moment-curve slope parameter $\partial C_m/\partial C_L$ is shown at two lift coefficients in figure 17. The nonlinearity of the variation of pitching-moment coefficient with lift coefficient (fig. 16) curtails the usefulness of data defining the pitching-moment characteristics in terms of the slope parameter $\partial C_m/\partial C_L$. The data of figure 17 illustrate, however, the general compressibility effects on the slope parameter $\partial C_m/\partial C_L$ for the lift coefficients shown, and indicate a general rearward movement of the aerodynamic center at high speeds for all angles of sweepback.

Downwash and Total-Pressure Surveys

Data on point downwash angles are given in figure 18 and on wake shapes in figures 19 and 20. The data on downwash angles presented herein are uncorrected for sting interference. As pointed out previously in the section entitled "CORRECTIONS AND PRECISION," the effect of sting interference on downwash angle is indicated to be appreciable at subsonic Mach numbers.

The flow in the region of the lowest yaw tube (0.125 wing semispan above chord plane of wing) on the inboard rake was affected to a large extent by the presence of the fuselage alone at angles of attack greater than 4°, as shown by the downwash data (fig. 18(a)) and the total-pressure data (figs. 19(b) and 19(d)). There was a negative downwash, or upwash, in the region of the lowest yaw tube on the inboard rake at angles of attack in the approximate angle-of-attack range from 4° to 12° for the fuselage-alone configuration. The downwash was positive in the region of the middle and uppermost yaw tubes on the inboard rake for the fuselage-alone configuration. The downwash at the outboard rake was only moderately affected by the presence of the fuselage alone, and the slope $d\epsilon/d\alpha$ was generally negative throughout the angle-of-attack range (fig.18(b)). The fuselage-alone configuration had essentially no effect on the total pressure at the outboard rake (fig. 20).

For the wing-fuselage configurations, the downwash-angle variations in the vicinity of the lowest yaw tube on the inboard rake were generally very irregular at the higher angles of attack at subsonic Mach numbers and throughout the angle-of-attack range at a Mach number of 1.2 (fig. 18(a)) and the total-pressure losses were large (fig. 19). The downwash for the wing-fuselage configurations varied more regularly with angle of attack in the region of the middle and uppermost yaw tubes on the inboard rake and in the region of all yaw tubes on the outboard rake than in the region of the lowest yaw tube on the inboard rake (figs. 18(a) and 18(b)). The downwash and total-pressure data for the outboard rake (figs. 18(b) and 20) are more indicative of the influence of the wing on the flow than the corresponding data for the inboard rake which were also affected by the modification of the flow by the fuselage. In general, the mean rate of change of downwash angle with angle of attack for the wing-fuselage configurations decreased with an increase in sweep angle. Exceptions to this statement occurred mainly where the flow was strongly influenced by the presence of the fuselage and for a sweepback angle of 60° at a Mach number of 1.2.

The extent of the wake above the chord plane of the wing was much greater for the wing-fuselage configuration with unswept wing than for the configurations with sweepback angles of 35°, 45°, and 60° (figs. 19 and 20). The magnitude of the total-pressure losses as obtained in

these tests was also usually greatest for the unswept configuration. A few exceptions to this statement were noted. For angles of attack less than 8° there was small difference in the upper extent of the wake at both rakes for the configurations with sweepback angles of 35°, 45°, and 60°. At angles of attack greater than 8° the configuration with a sweepback angle of 35° showed a greater wake extent at the outboard rake than the configurations with higher sweepback angle. This was also true in some but not all instances for the inboard rake. The maximum loss in total pressure was not obtained in many cases, so that there was appreciable variation as regards maximum measured loss with change in sweep angle.

Base-Pressure Coefficient

The base-pressure coefficient generally increased with an increase in Mach number at subsonic speeds for all the wing-fuselage configurations and for the fuselage alone (fig. 21). At an angle of attack of 12°, however, the base-pressure coefficient for the unswept configuration decreased with Mach number. At a Mach number of 1.2 the base-pressure coefficient was generally somewhat less than at the highest subsonic test Mach numbers.

At subsonic speeds sweepback angle had relatively small effect on the base-pressure coefficient except at the highest angles of attack where sweepback angles in the vicinity of zero sweep caused a decrease in the base-pressure coefficient. At a Mach number of 1.2, increasing the sweepback angle resulted first in a decrease in base-pressure coefficient and then in an increase in base-pressure coefficient.

CONCLUSIONS

An investigation was made in the Langley 8-foot high-speed tunnel of the effects of wing sweepback angle (0°, 35°, 45°, and 60°) on the characteristics of a wing-fuselage configuration without tail surfaces. Lift, drag, and pitching-moment coefficients were obtained. Downwash and total-pressure surveys at two spanwise stations were made in the region of a probable tail location. All the wings had NACA 65A006 airfoil sections parallel to the model plane of symmetry, an area of 1 square foot, an aspect ratio of 4, and a taper ratio of 0.6. The tests were made at subsonic Mach numbers up to approximately 0.95 and at one supersonic Mach number of 1.2. The Reynolds number based on the mean aerodynamic chord was 2×10^6 at the maximum subsonic speed. The following conclusions are indicated:

1. An increase in sweepback angle reduced the adverse compressibility effects on lift, drag, pitching moment, and maximum lift-drag ratio.

2. At Mach numbers from approximately 0.88 to 0.95, the maximum lift-drag ratio increased with an increase in sweepback angle up to 45° and then decreased between sweep angles of 45° and 60°. At a Mach number of 1.2 the maximum lift-drag ratio increased with an increase in sweepback angle up to the maximum sweep angle of 60°.

3. Abrupt, unstable changes in pitching-moment coefficients, which are associated with complete separation of the flow over the tip sections of sweptback wings, occurred with an increase in lift coefficient at subsonic Mach numbers for sweepback angles of 35°, 45°, and 60°. An increase in sweepback angle increased the severity of the unstable changes and reduced the lift coefficient at which these changes began.

4. In general, the mean rate of change of downwash angle with angle of attack decreased with an increase in sweepback angle. Exceptions to this statement occurred mainly where the flow was strongly influenced by the presence of the fuselage and for a sweepback angle of 60° at a Mach number of 1.2.

5. The upper extent of the wake above the chord plane of the wing and the magnitude of the total-pressure losses were much greater for an angle of sweepback of 0° than for angles of sweepback of 35°, 45°, and 60°. At moderate angles of attack there was little difference in the upper extent of the wake for angles of sweepback of 35°, 45°, and 60°.

Langley Aeronautical Laboratory
     National Advisory Committee for Aeronautics
          Langley Field, Va.

REFERENCES

1. Osborne, Robert S.: A Transonic-Wing Investigation in the Langley
    8-Foot High-Speed Tunnel at High Subsonic Mach Numbers and at a
    Mach Number of 1.2. Wing-Fuselage Configuration Having a Wing
    of 45° Sweepback, Aspect Ratio 4, Taper Ratio 0.6, and NACA 65A006
    Airfoil Section. NACA RM L50H08, 1950.

2. Henry, Beverly Z., Jr.: A Transonic Wing Investigation in the
    Langley 8-Foot High-Speed Tunnel at High Subsonic Mach Numbers
    and at a Mach Number of 1.2. Wing-Fuselage Configuration Having
    a Wing of 35° Sweepback, Aspect Ratio 4, Taper Ratio 0.6, and
    NACA 65A006 Airfoil Section. NACA RM L50J09, 1950.

3. Cahn, Maurice S., and Bryan, Carroll R.: A Transonic-Wing Investi-
    gation in the Langley 8-Foot High-Speed Tunnel at High Subsonic
    Mach Numbers and at a Mach Number of 1.2. Wing-Fuselage Configu-
    ration Having a Wing of 0° Sweepback, Aspect Ratio 4.0, Taper
    Ratio 0.6, and NACA 65A006 Airfoil Section. NACA RM L51A02, 1951.

4. Wood, Raymond B., and Fleming, Frank F.: A Transonic-Wing Investi-
    gation in the Langley 8-Foot High-Speed Tunnel at High Subsonic
    Mach Numbers and at a Mach Number of 1.2. Wing-Fuselage Configu-
    ration Having a Wing of 60° Sweepback, Aspect Ratio 4, Taper
    Ratio 0.6, and an NACA 65A006 Airfoil Section. NACA RM L50J25,
    1951.

5. Donlan, Charles J., Myers, Boyd C., II, and Mattson, Axel T.: A
    Comparison of the Aerodynamic Characteristics at Transonic Speeds
    of Four Wing-Fuselage Configurations as Determined from Different
    Test Techniques. NACA RM L50H02, 1950.

6. Ritchie, Virgil S., Wright, Ray H., and Tulin, Marshall P.: An
    8-Foot Axisymmetrical Fixed Nozzle for Subsonic Mach Numbers up to
    0.99 and for a Supersonic Mach Number of 1.2. NACA RM L50A03a,
    1950.

7. Osborne, Robert S.: High-Speed Wind-Tunnel Investigation of the
    Longitudinal Stability and Control Characteristics of a $\frac{1}{16}$ - Scale
    Model of the D-558-2 Research Airplane at High Subsonic Mach
    Numbers and at a Mach Number of 1.2. NACA RM L9C04, 1949.

8. Diederich, Franklin W.: A Simple Approximate Method for Obtaining
    Spanwise Lift Distributions over Swept Wings. NACA RM L7I07,
    1948.

9. De Young, John: Theoretical Additional Span Loading Character-
   istics of Wings with Arbitrary Sweep, Aspect Ratio, and Taper
   Ratio. NACA TN 1491. 1947.

10. Lange, Roy H., Whittle, Edward F., Jr., and Fink, Marvin P.:
    Investigation at Large Scale of the Pressure Distribution and
    Flow Phenomena over a Wing with the Leading Edge Swept Back 47.5°
    Having Circular-Arc Airfoil Sections and Equipped with Drooped-
    Nose and Plain Flaps. NACA RM L9G15, 1949.

11. Anderson, Adrien E.: Chordwise and Spanwise Loadings Measured at
    Low Speed on Large Triangular Wings. NACA RM A9B17, 1949.

12. Cahill, Jones F., and Gottlieb, Stanley M.: Low-Speed Aerodynamic
    Characteristics of a Series of Swept Wings Having NACA 65A006
    Airfoil Sections. NACA RM L50F16, 1950.

13. Fisher, Lewis R.: Approximate Corrections for the Effects of
    Compressibility on the Subsonic Stability Derivatives of Swept
    Wings. NACA TN 1854, 1949.

TABLE I

AIRFOIL AND FUSELAGE ORDINATES

FUSELAGE

NACA 65A006 AIRFOIL
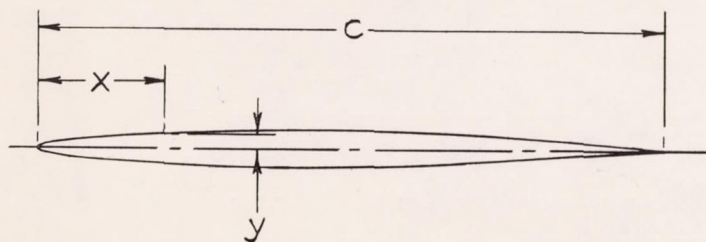
x/c	y/c	x/c	y/c
0	0	0.40	0.02996
.005	.00464	.45	.02992
.0075	.00563	.50	.02925
.0125	.00718	.55	.02793
.025	.00981	.60	.02602
.050	.01313	.65	.02364
.075	.01591	.70	.02087
.10	.01824	.75	.01775
.15	.02194	.80	.01437
.20	.02474	.85	.01083
.25	.02687	.90	.00727
.30	.02842	.95	.00370
.35	.02945	1.00	.00013

L.E. radius = 0.00229c
T.E. radius = 0.00014c
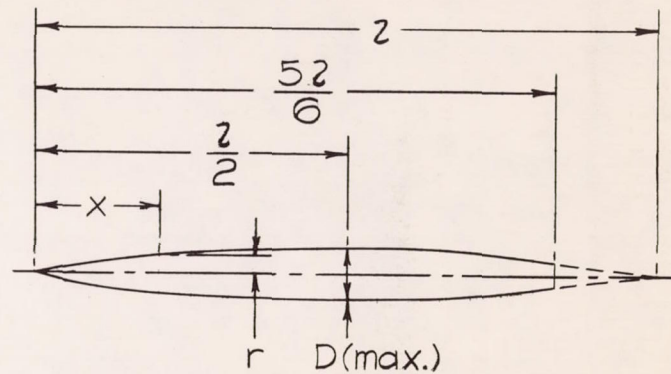
ORDINATES			
x/l	r/l	x/l	r/l
0.0050	0.00231	0.4500	0.04143
.0075	.00298	.5000	.04167
.0125	.00428	.5500	.04130
.0250	.00722	.6000	.04024
.0500	.01205	.6500	.03842
.0750	.01613	.7000	.03562
.1000	.01971	.7500	.03128
.1500	.02593	.8000	.02526
.2000	.03090	.8333	.02083
.2500	.03465	.8500	.01852
.3000	.03741	.9000	.01125
.3500	.03933	.9500	.00439
.4000	.04063	1.0000	0

L.E. radius = 0.0005l
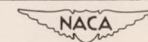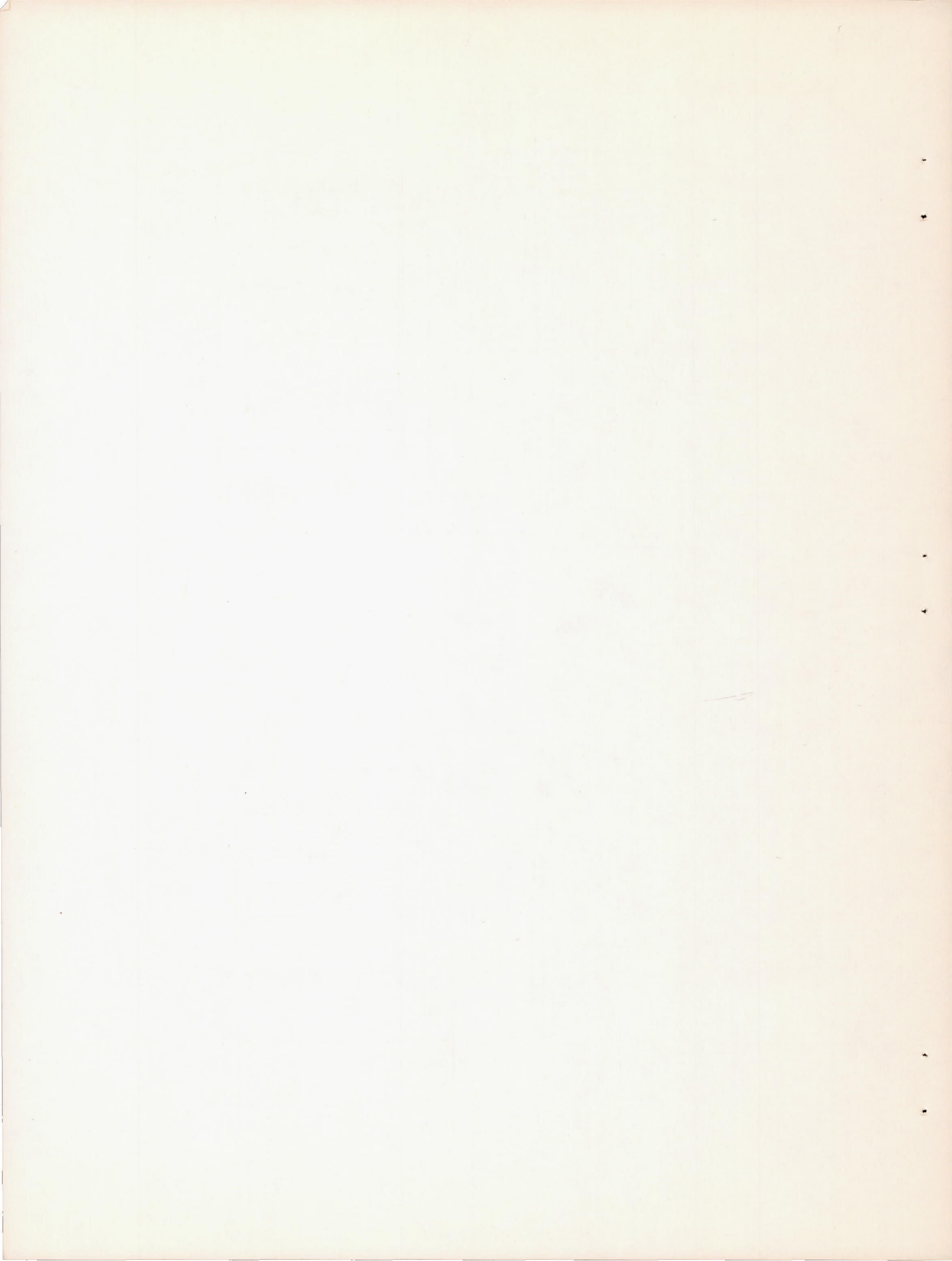
Figure 1.- Method of model installation in Langley 8-foot high-speed
tunnel for present tests.
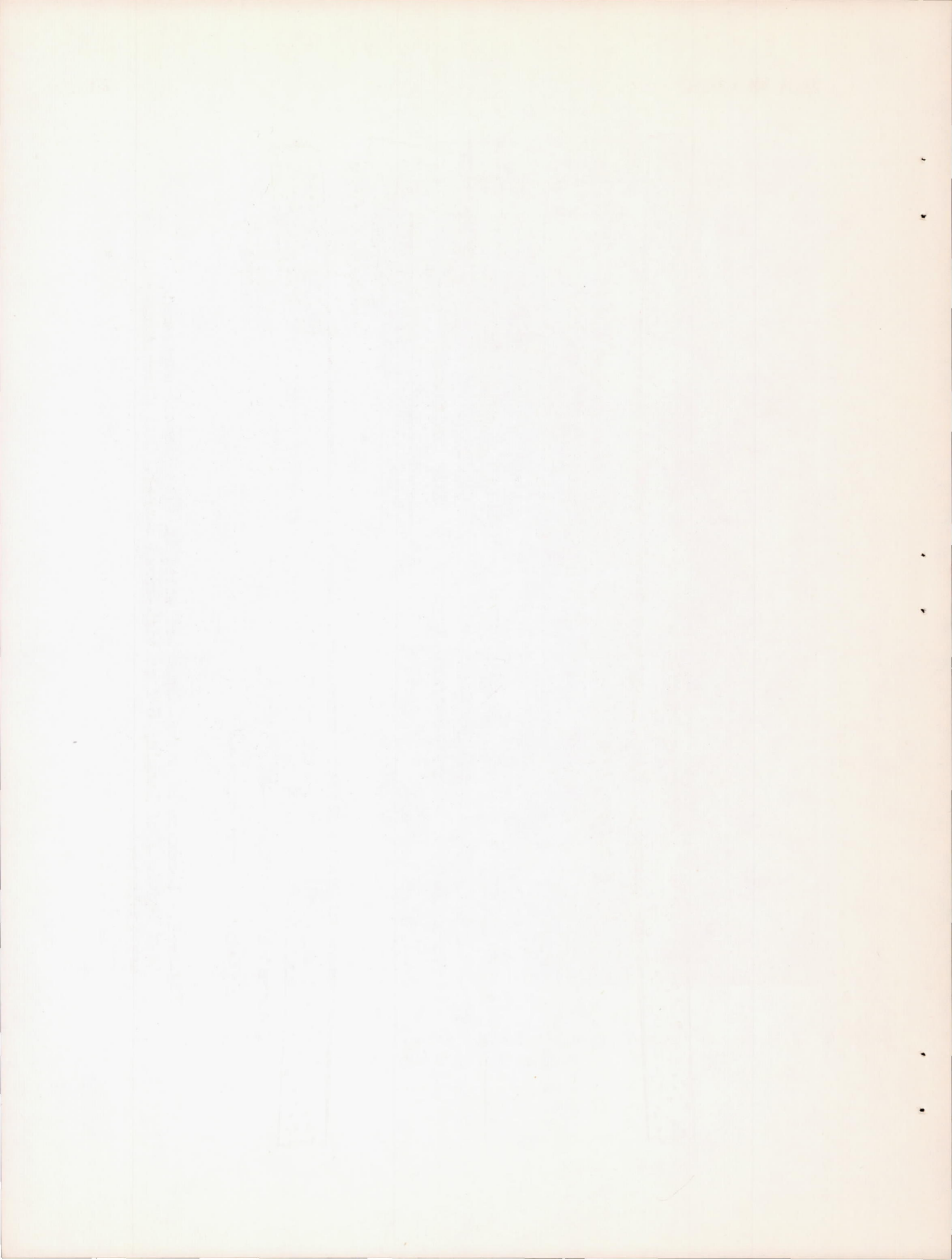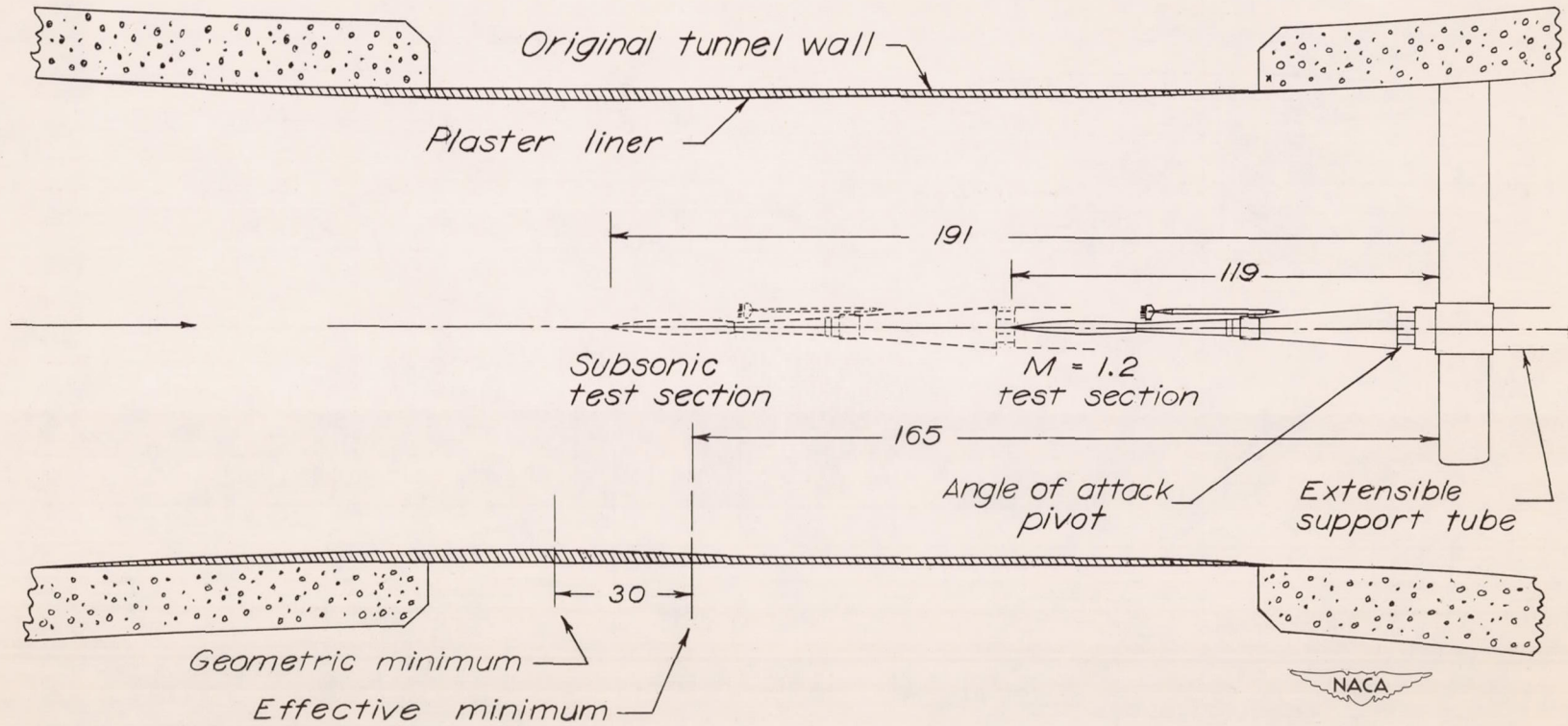
Figure 2.- Location of sting-supported model in subsonic and supersonic test sections of Langley 8-foot high-speed tunnel. All dimensions are in inches.

Wing:
Section (parallel to model plane of symmetry) NACA 65A006
Aspect ratio 4
Taper ratio 0.6
Area, sq ft 1.0
Dihedral, deg 0
Geometric twist, deg 0

Position of wing on fuselage:
Incidence, deg 0
Location of chord plane from
fuselage axis, in. 0

Figure 3.- Model configurations tested. All dimensions are in inches
except as noted.

Base-pressure orifice

Model plane of symmetry

1.0

3.5

Plan view

1.37

.5
.5
.5
.5
.5
.5

4.5

3.0

Wing-chord plane

1.5

NACA

Fuselage

Sting

Side elevation

Figure 4.- Location of rakes used for downwash and total-pressure surveys.
All dimensions are in inches.
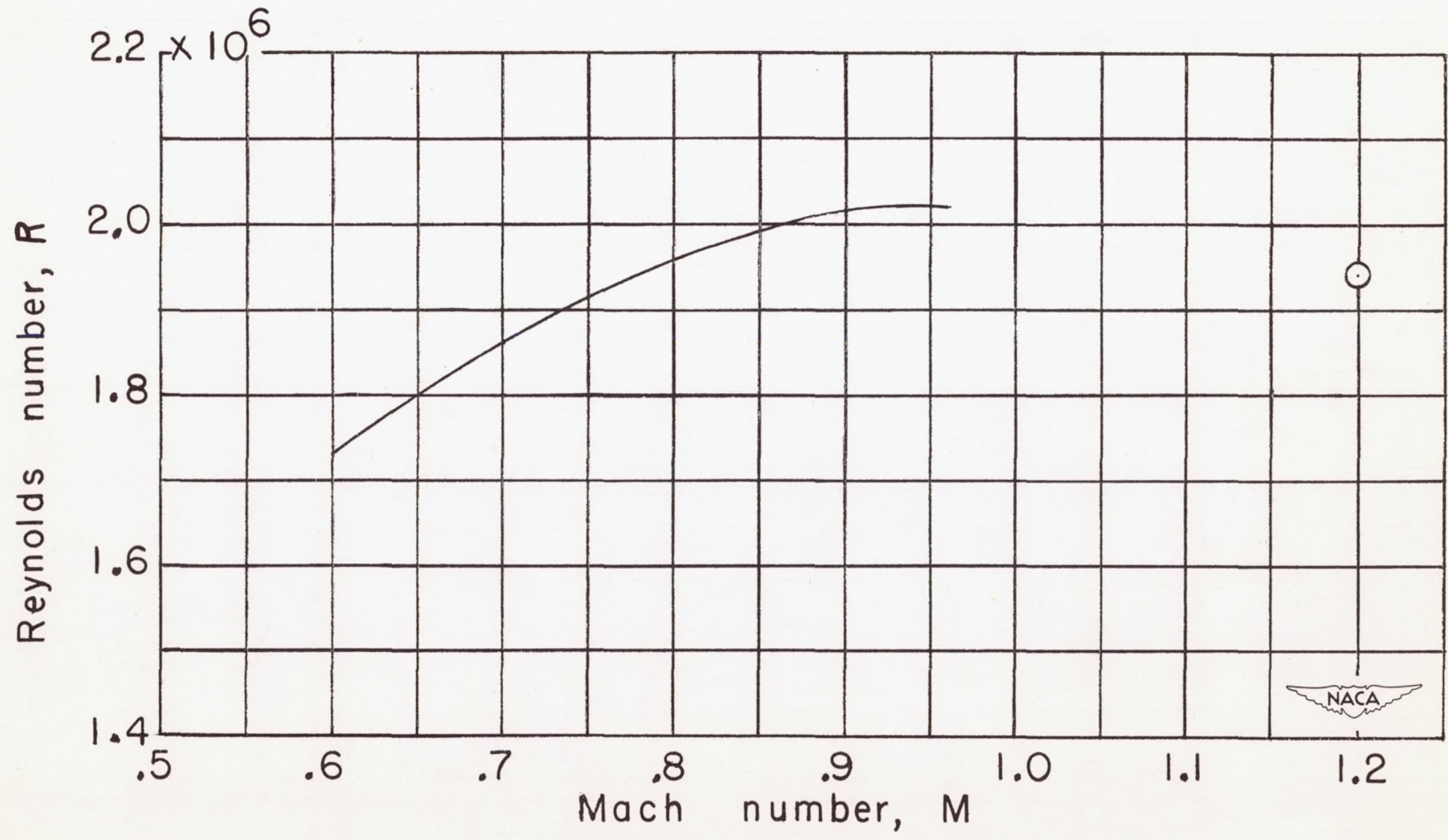
Figure 5.- Variation of Reynolds number with Mach number in the investigation of sweepback angle in the Langley 8-foot high-speed tunnel. c' = 6.125 inches.
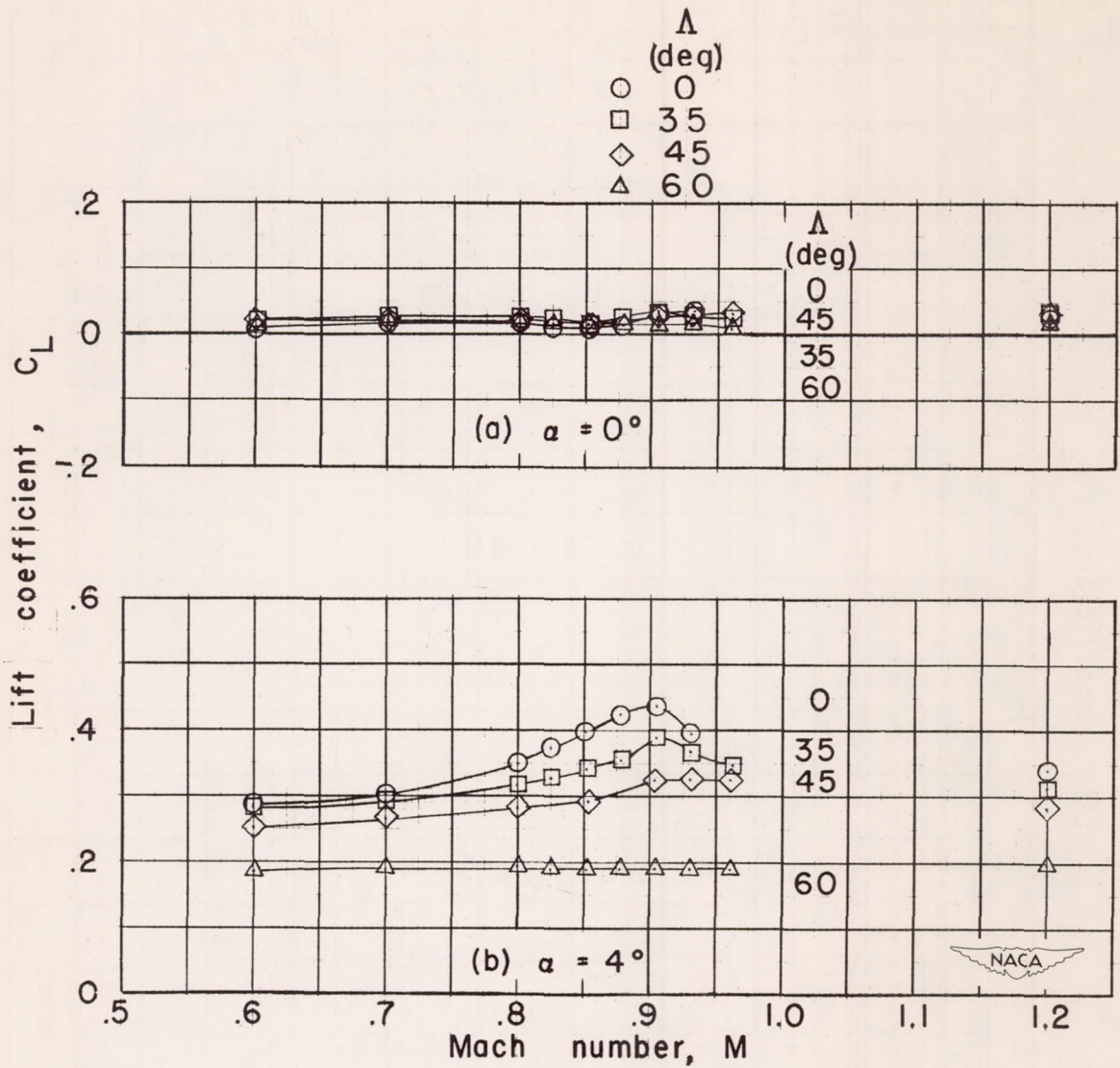
Figure 6.- Variation of lift coefficient with Mach number at various angles of sweepback. Wing-fuselage configuration; NACA 65A006 airfoil section, A = 4, λ = 0.6.
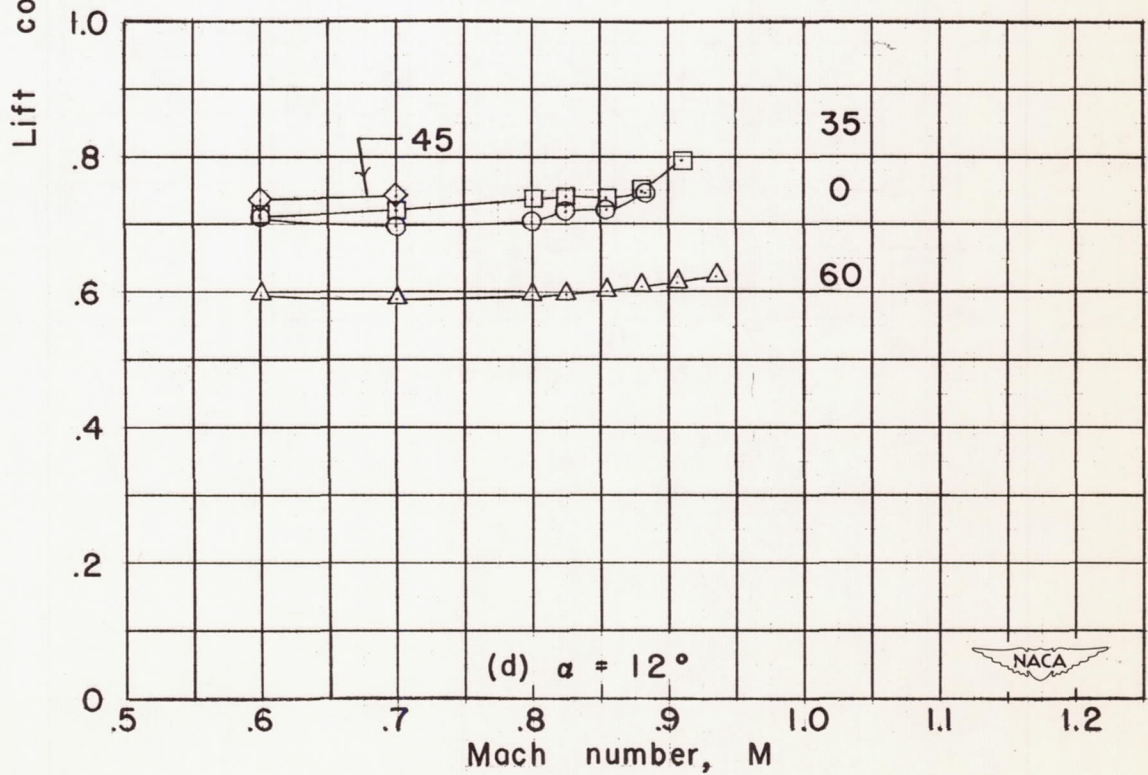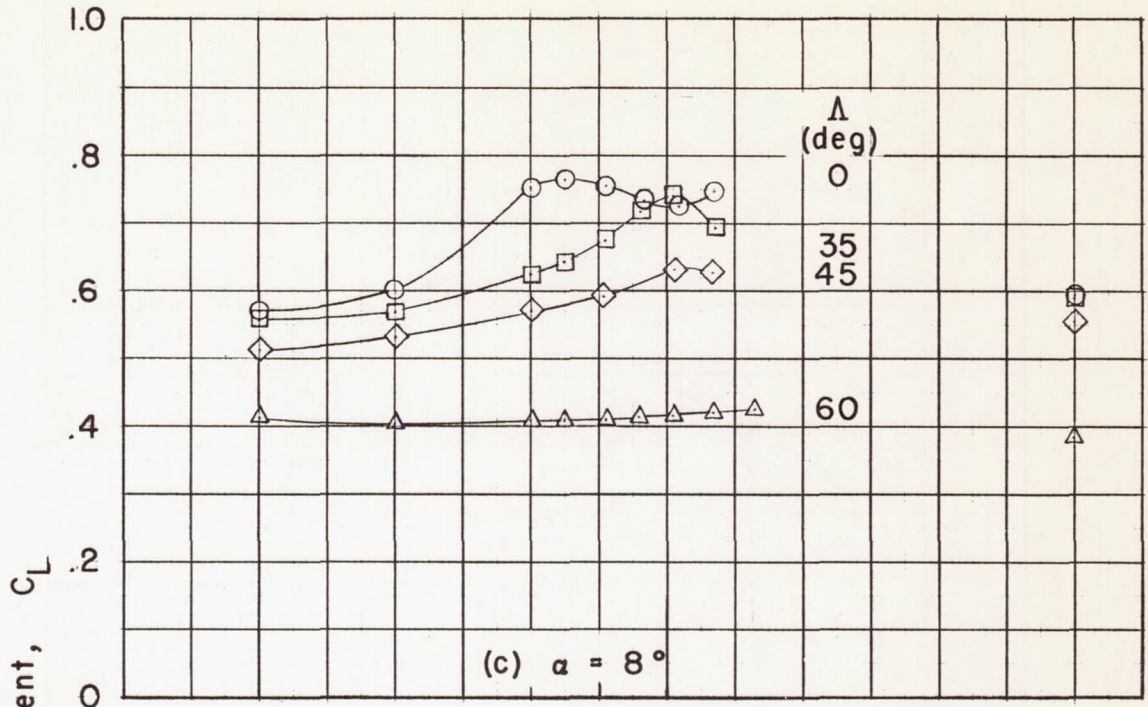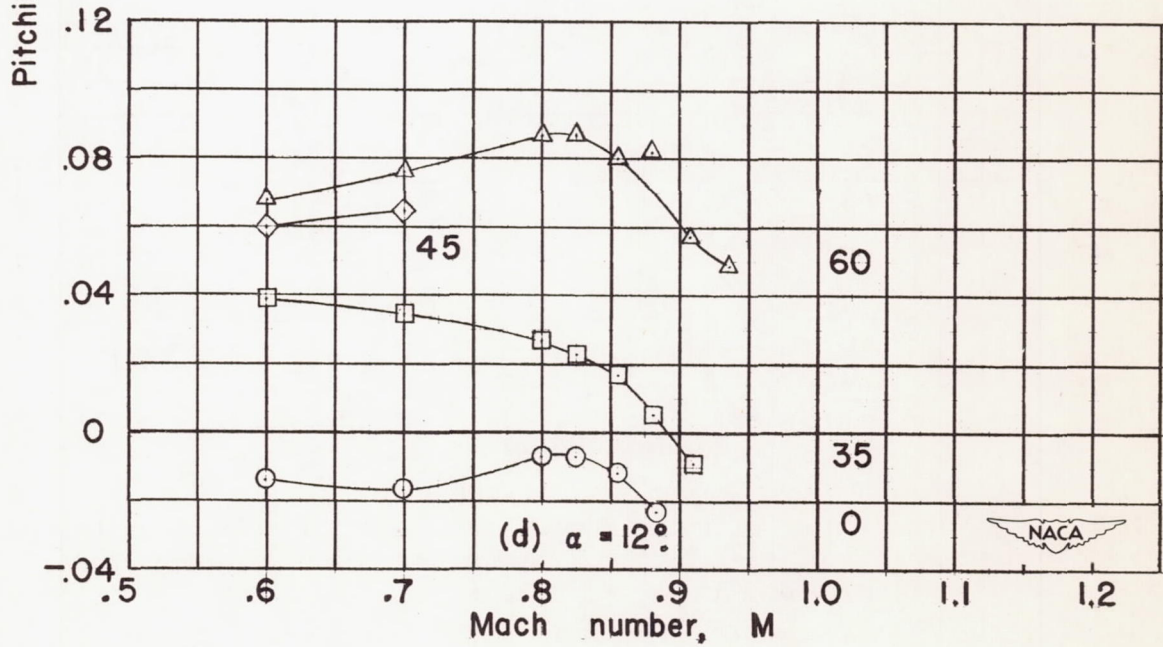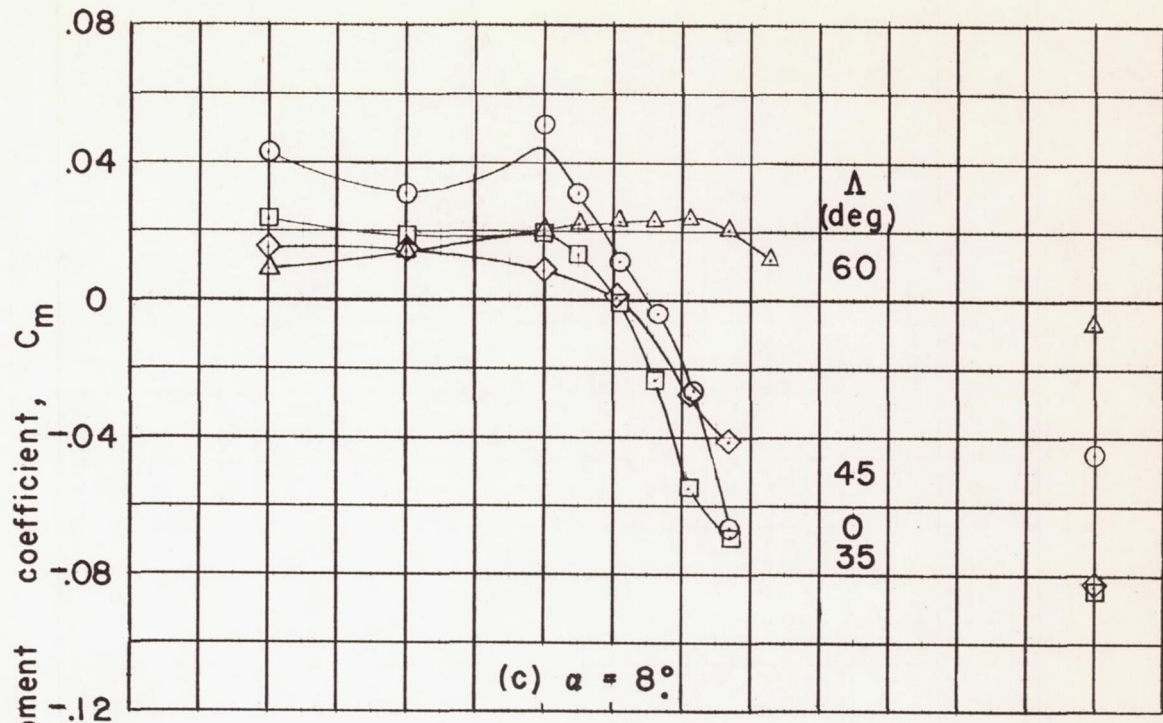
Figure 6.- Concluded.
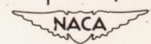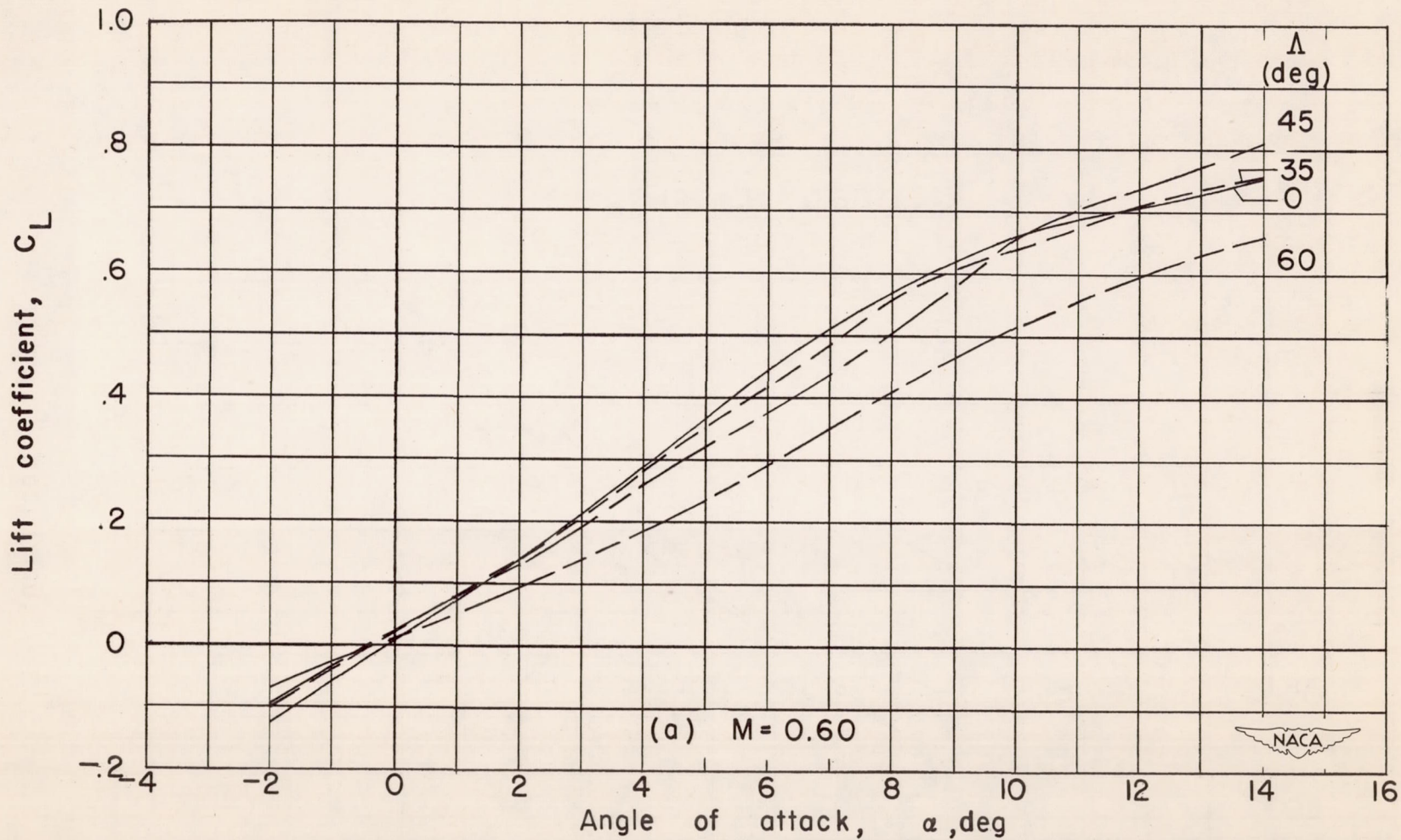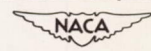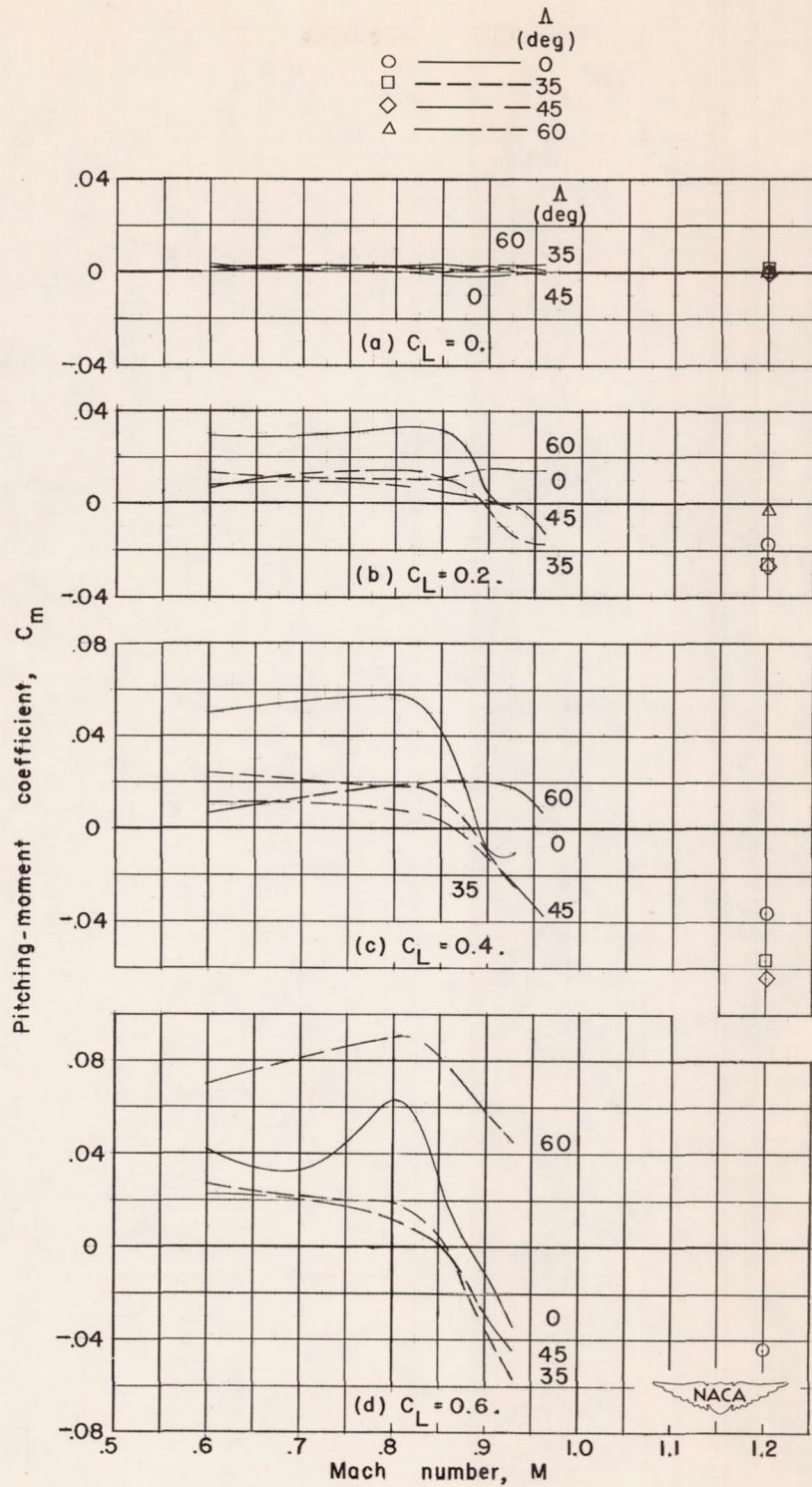
Figure 7.- Variation of lift coefficient with angle of attack at various
angles of sweepback. Wing-fuselage configuration, NACA 65A006 airfoil
section, A = 4, λ = 0.6.

(b)   M = 0.90.
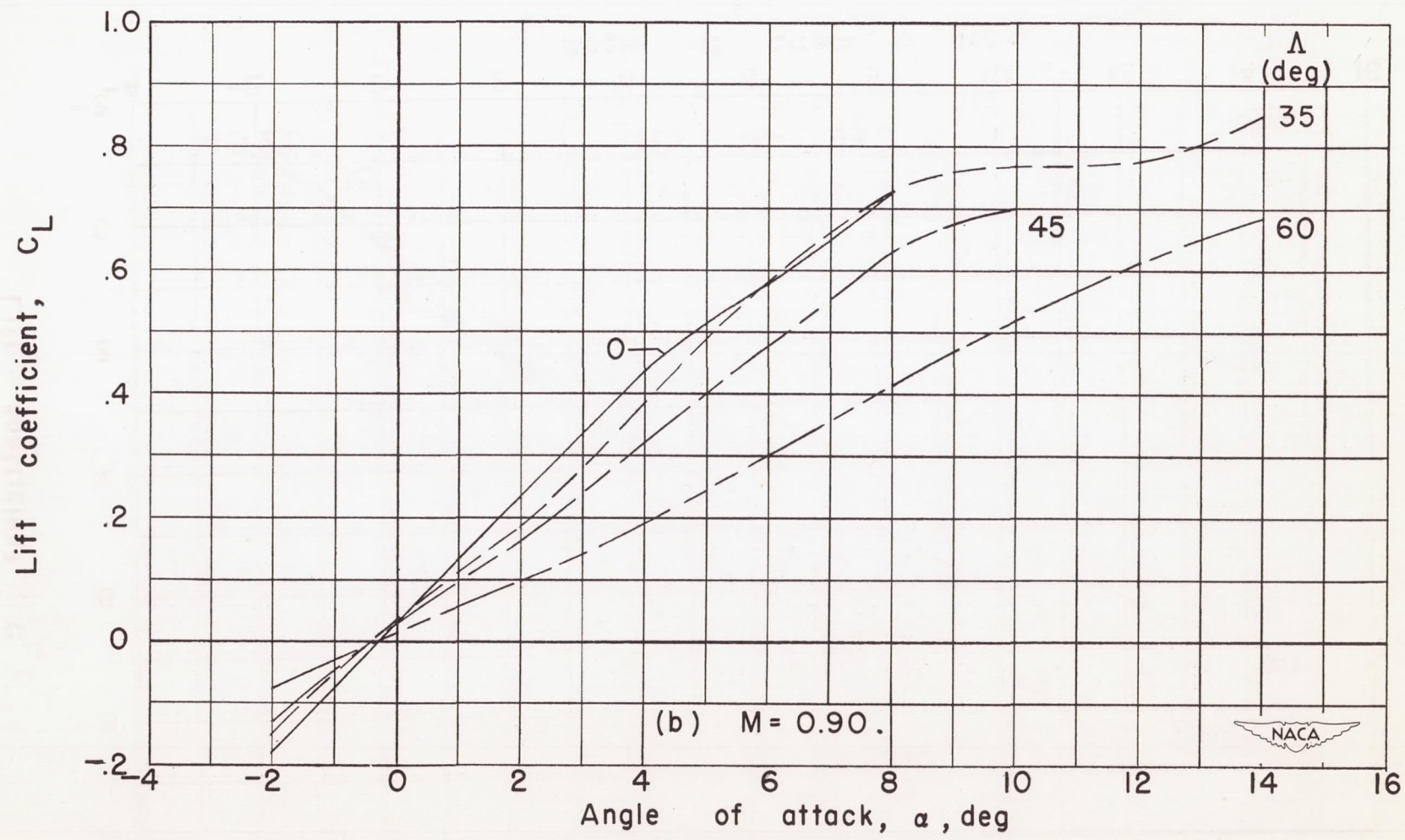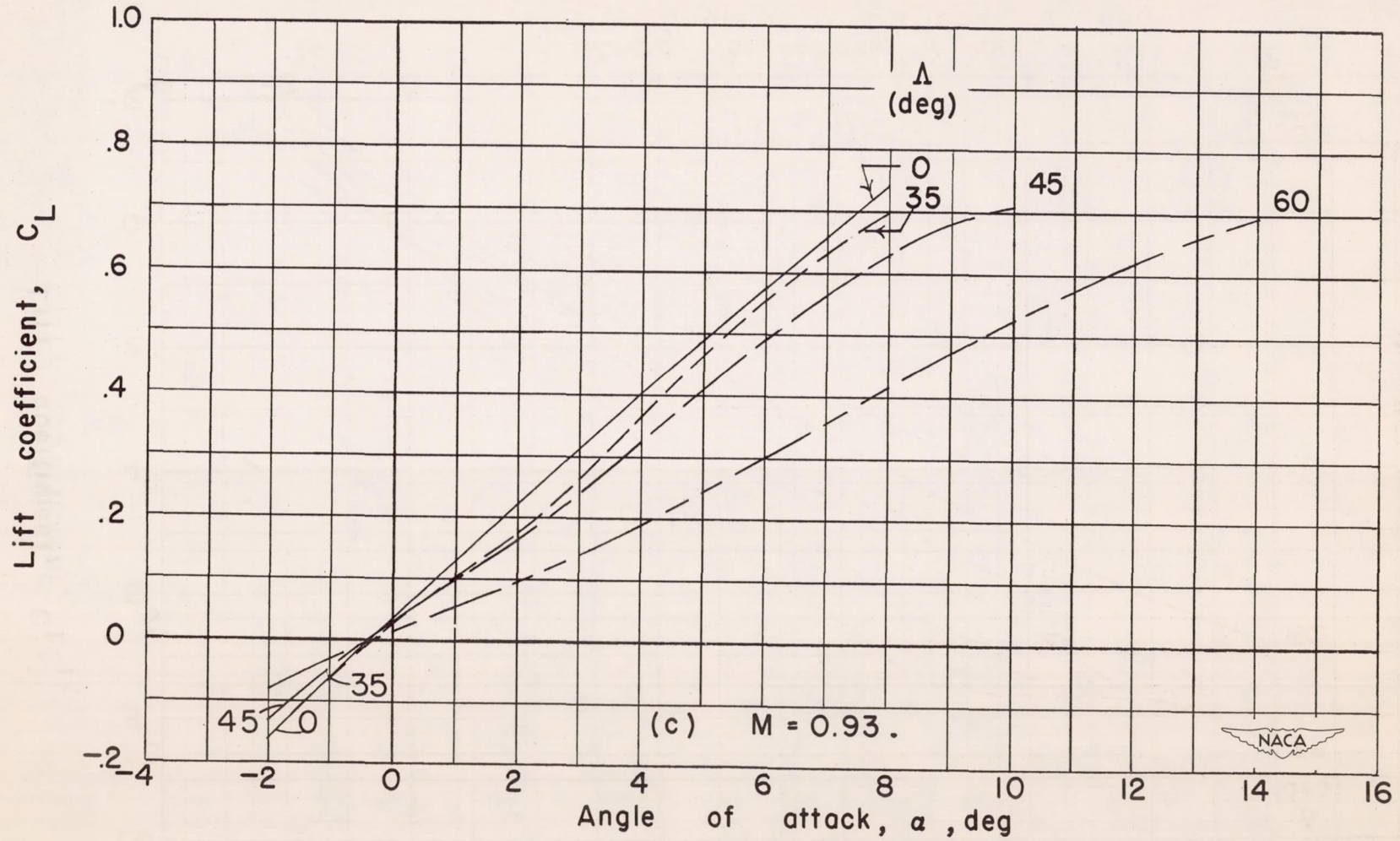
Figure 7.- Continued.

Figure 7.- Continued.

(d)   M = 1.2 .
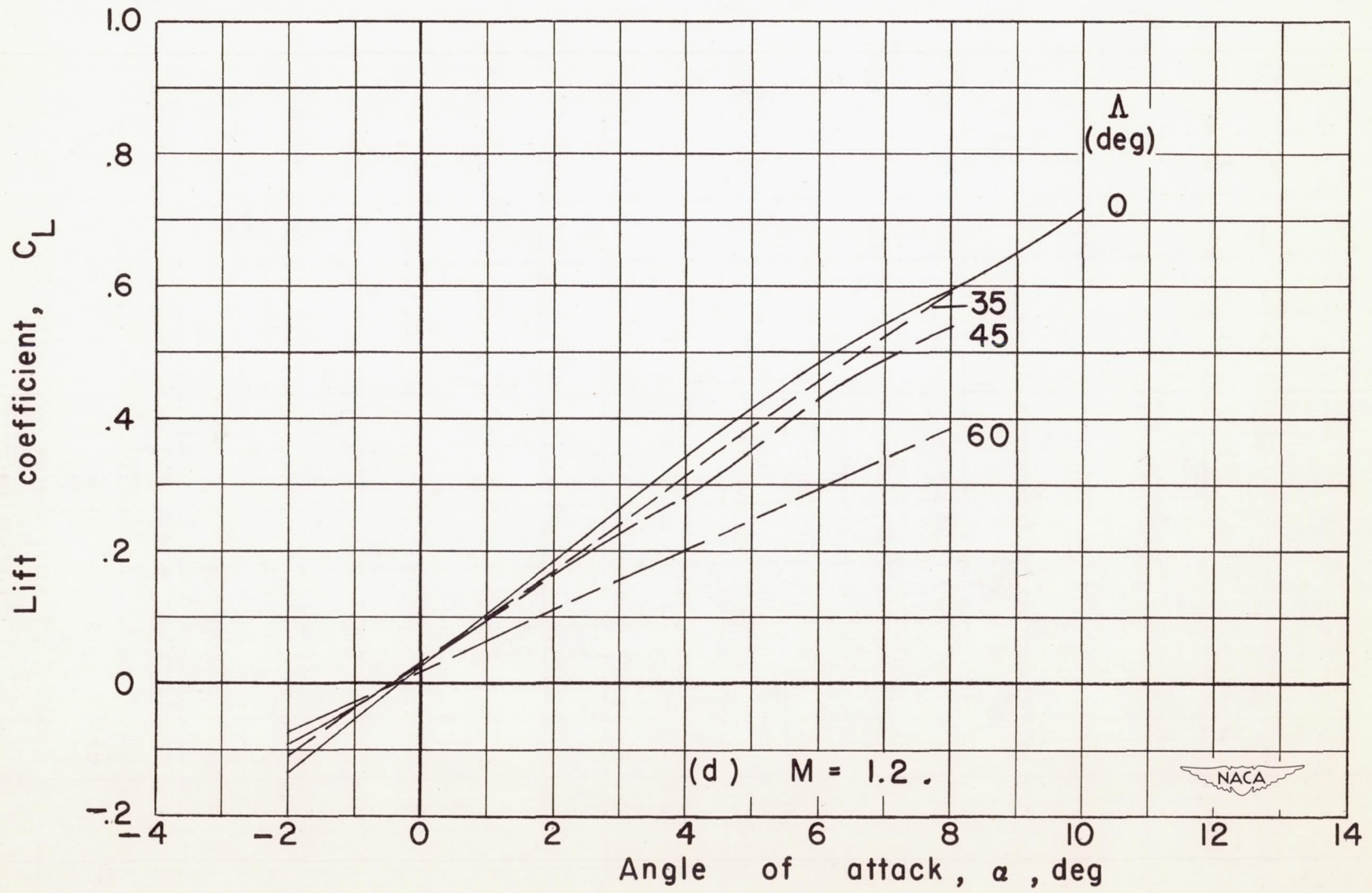
Figure 7.- Concluded.
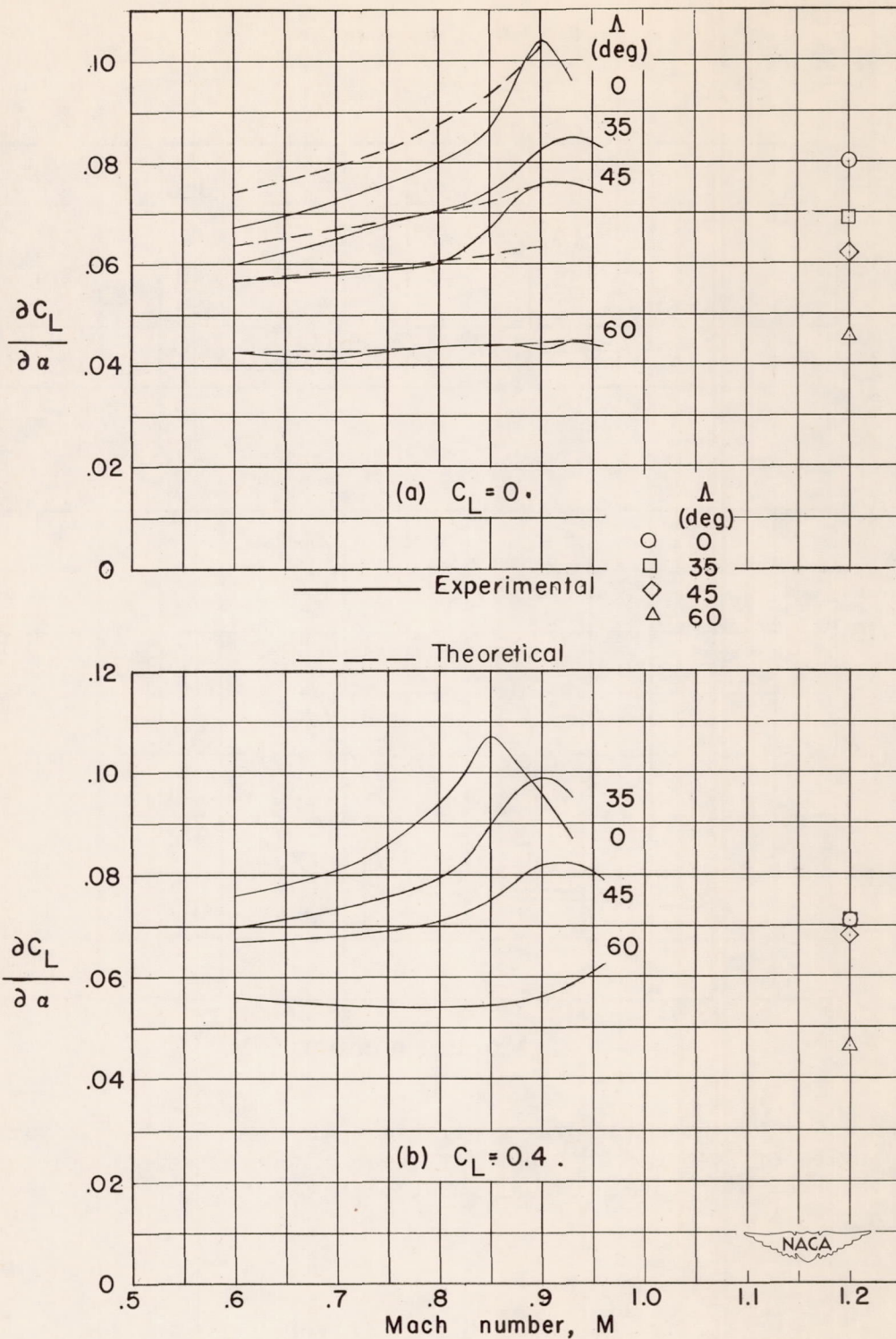
Figure 8.- Variation of lift-curve slope $\dfrac{\partial C_L}{\partial \alpha}$ with Mach number at various angles of sweepback. Wing-fuselage configuration; NACA 65A006 airfoil section, $A = 4$, $\lambda = 0.6$.
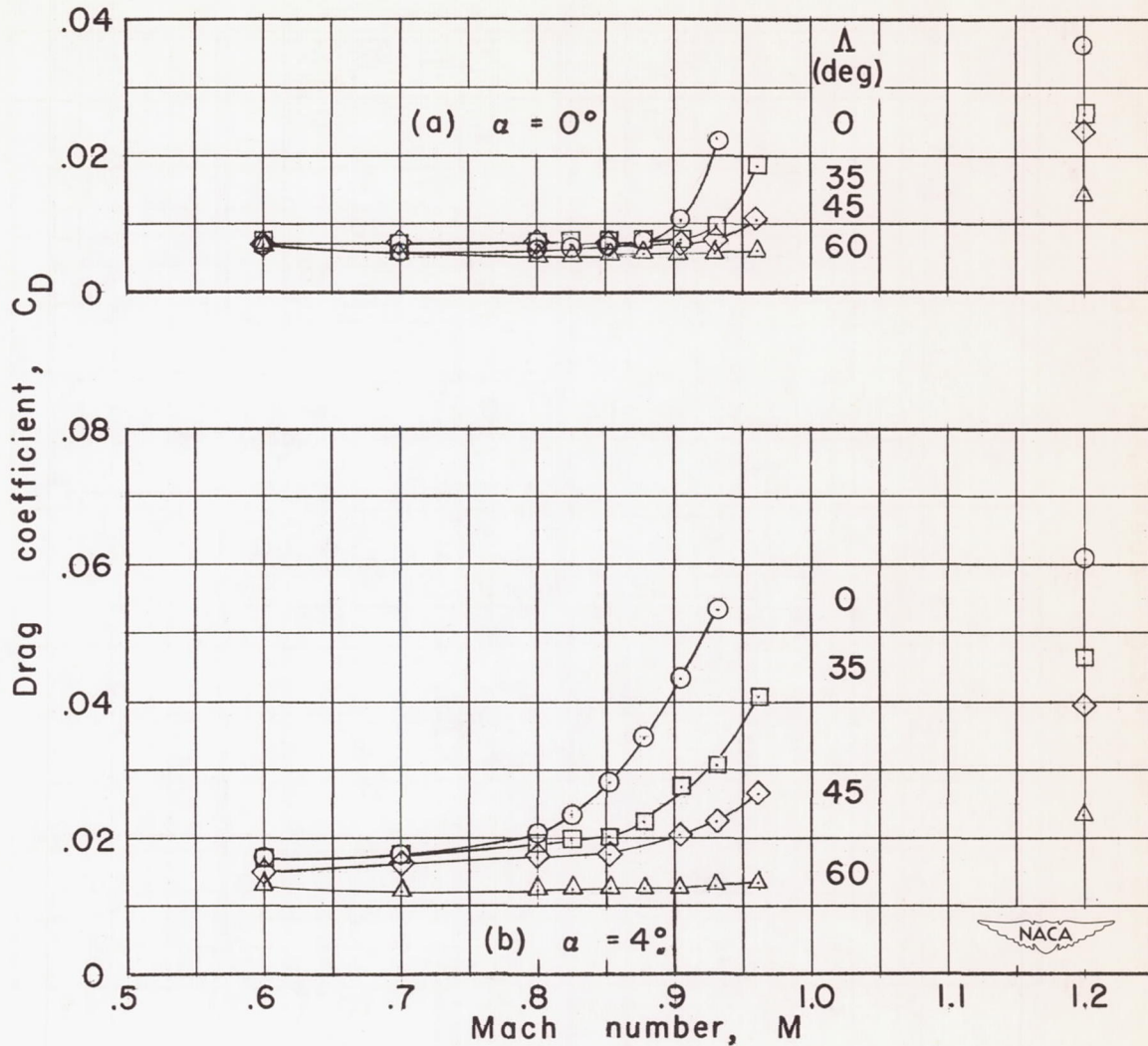
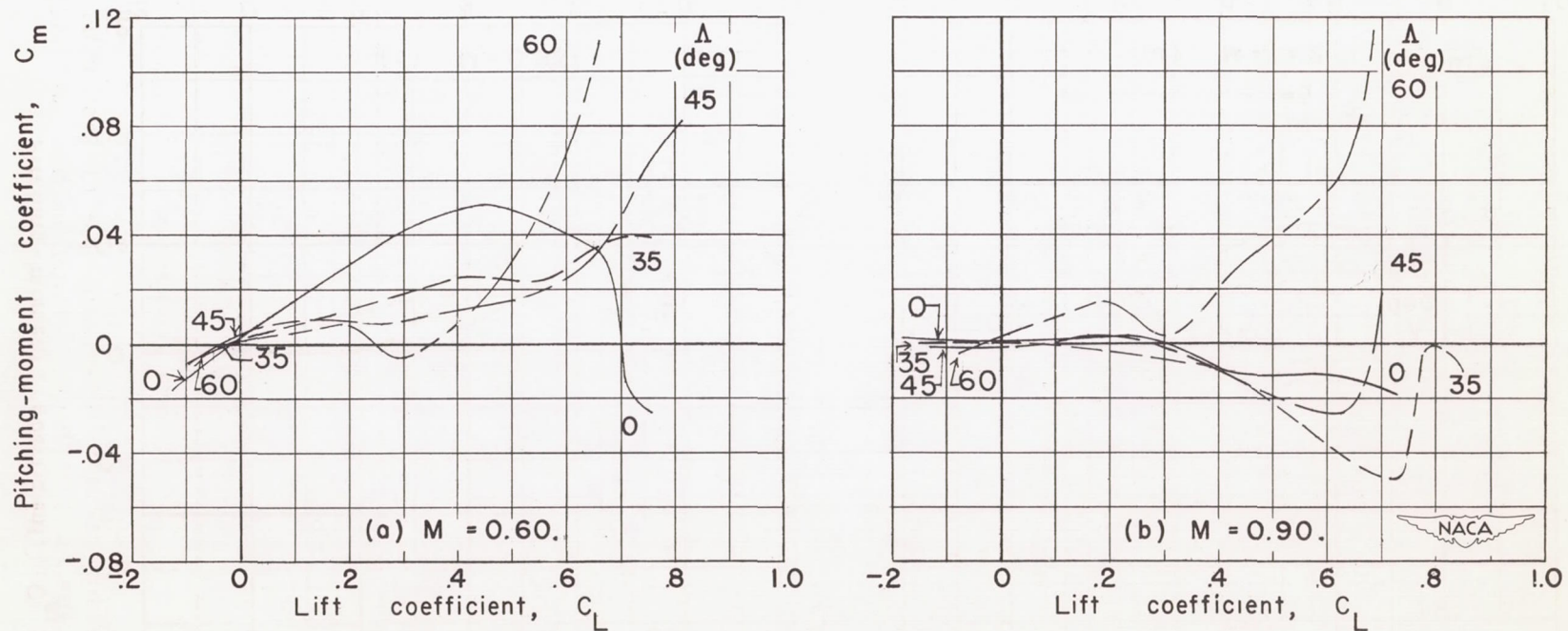Figure 9.- Variation of drag coefficient with Mach number at various
angles of sweepback. Drag coefficient uncorrected for sting inter-
ference; wing-fuselage configuration; NACA 65A006 airfoil section,
A = 4, λ = 0.6.
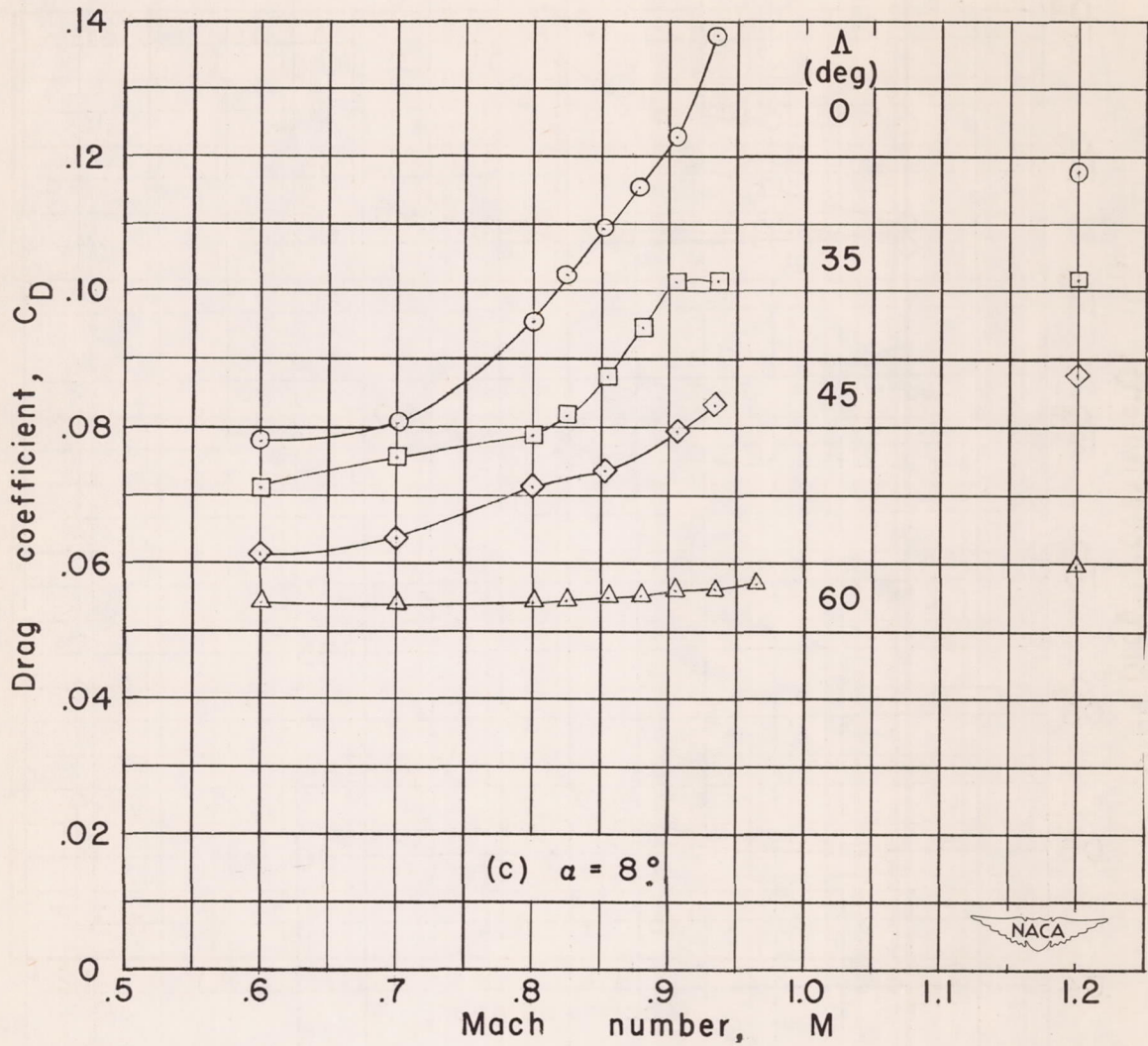
Figure 9.- Continued.
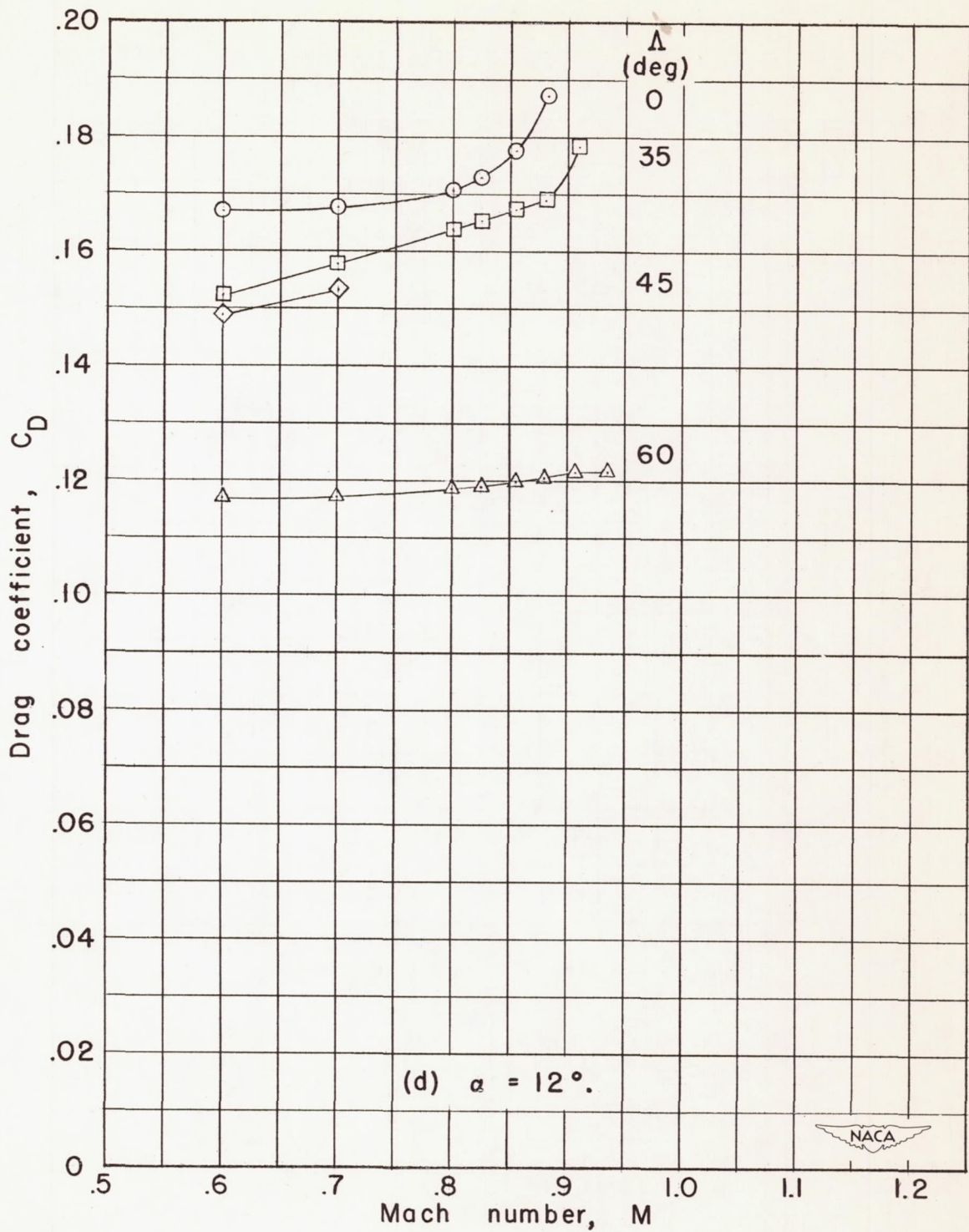
Figure 9.- Concluded.
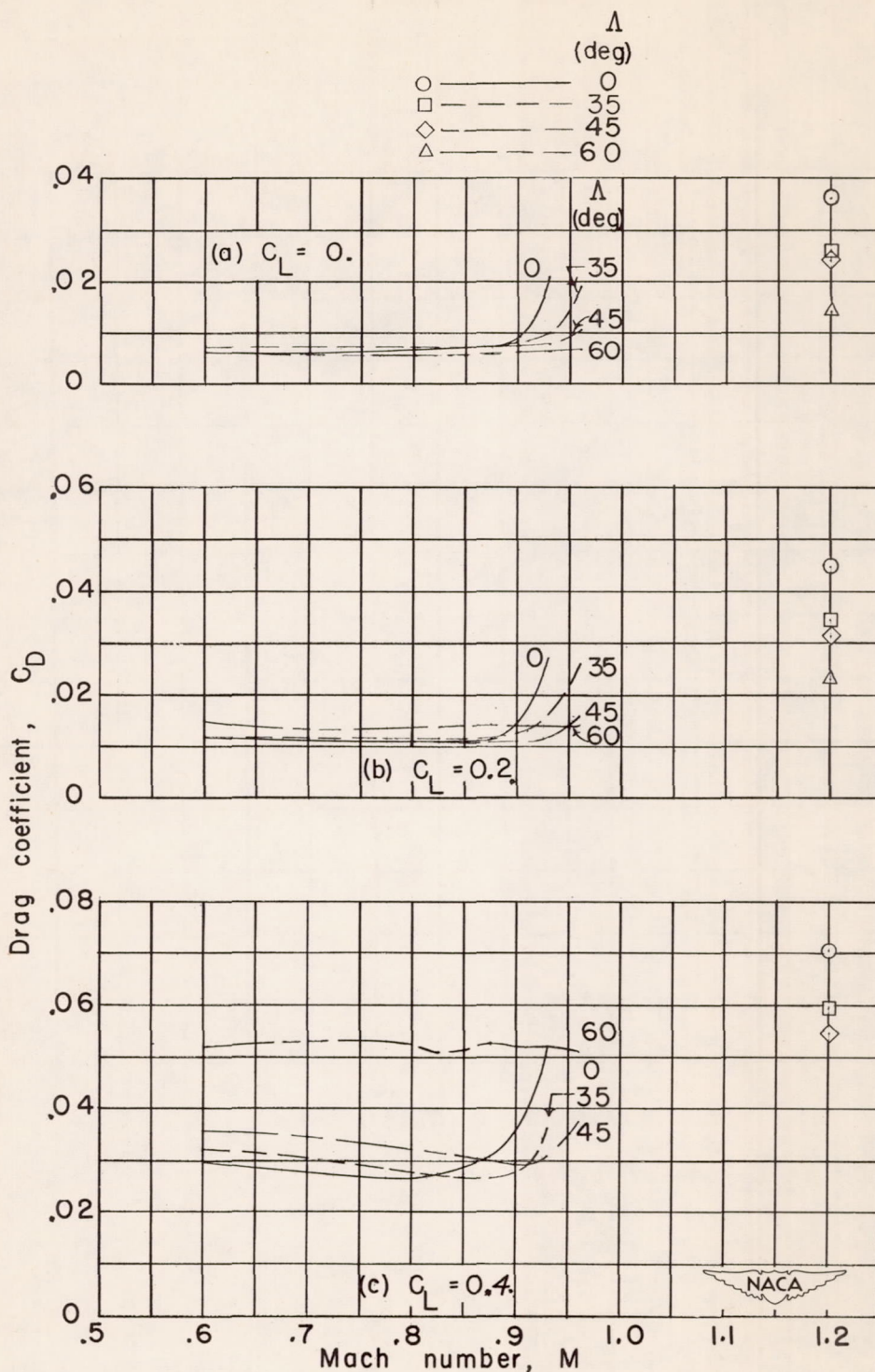
Figure 10.- Variation of drag coefficient with Mach number at various angles of sweepback. Drag coefficient uncorrected for sting interference; wing-fuselage configuration; NACA 65A006 airfoil section, $A = 4$, $\lambda = 0.6$.
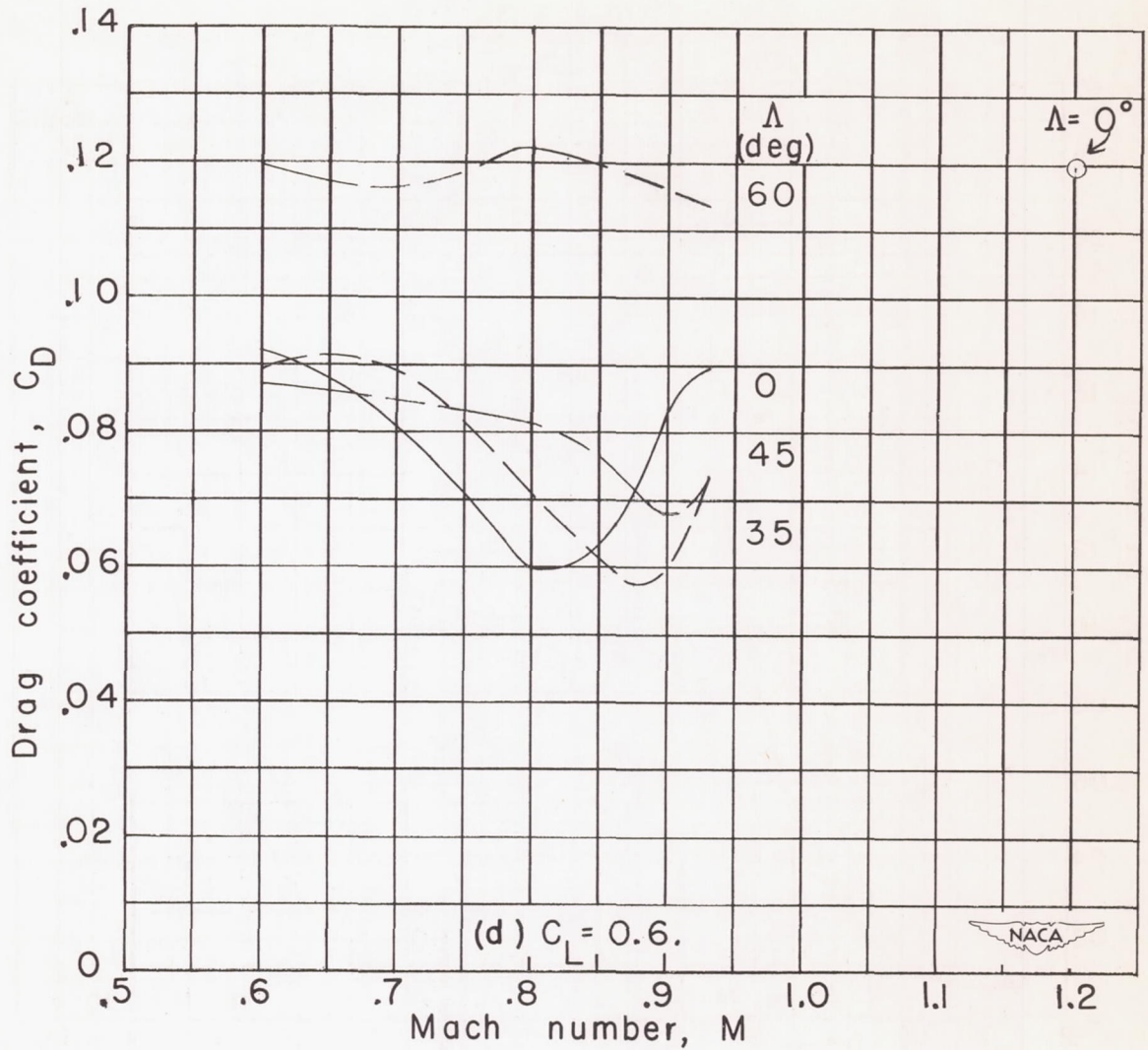
Figure 10.- Concluded.
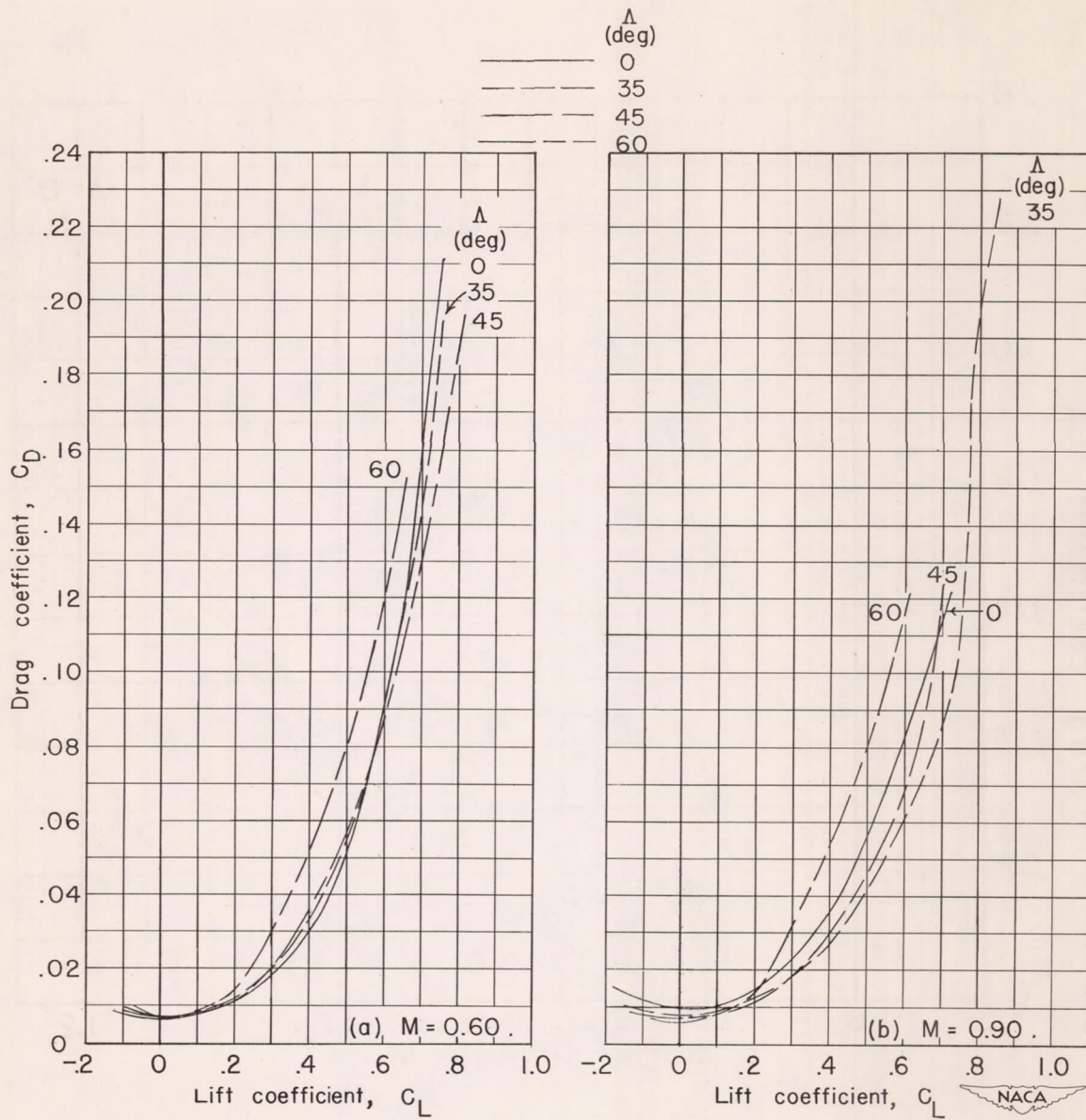
Figure 11.- Variation of drag coefficient with lift coefficient at various angles of sweepback. Drag coefficient uncorrected for sting interference; wing-fuselage configuration; NACA 65A006 airfoil section, A = 4, λ = 0.6.
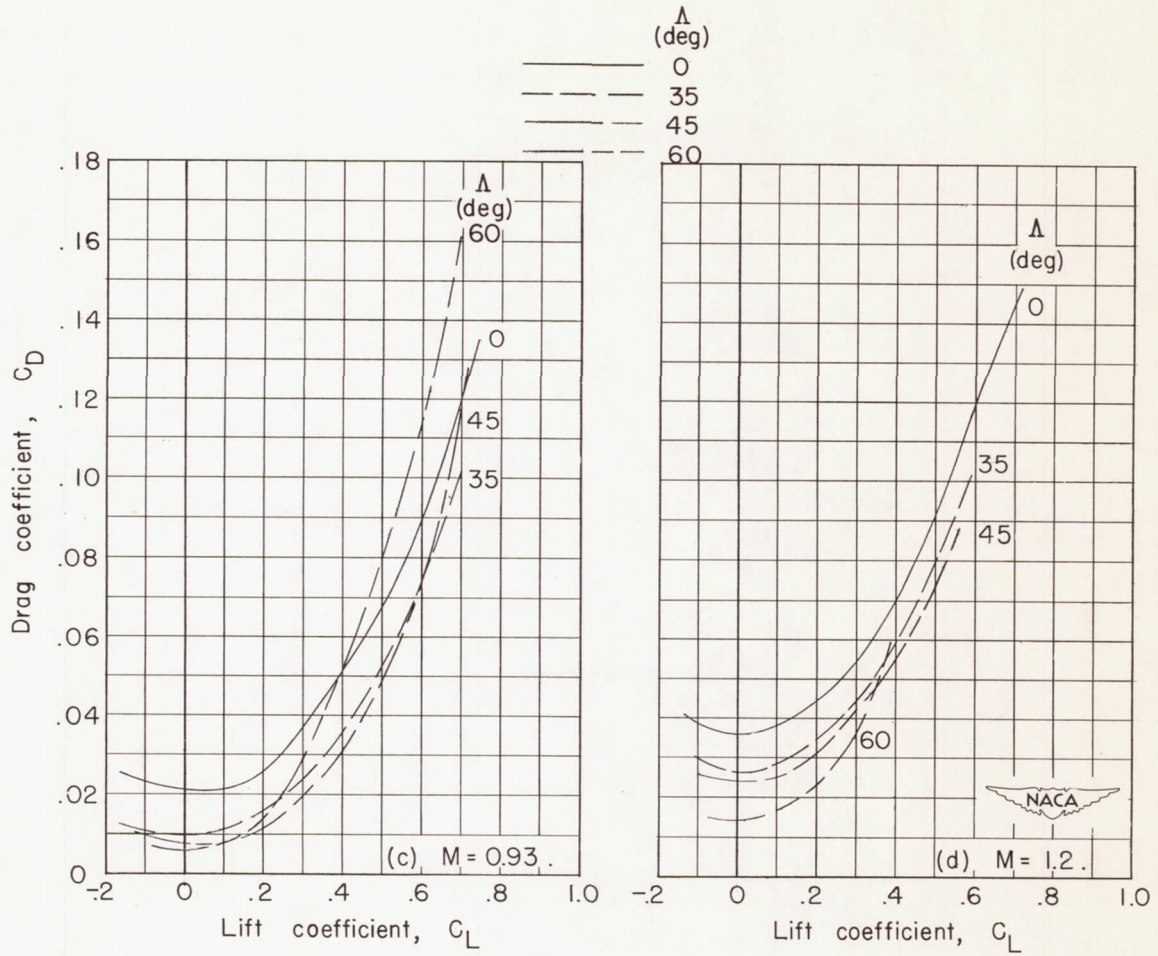
Figure 11.- Concluded.
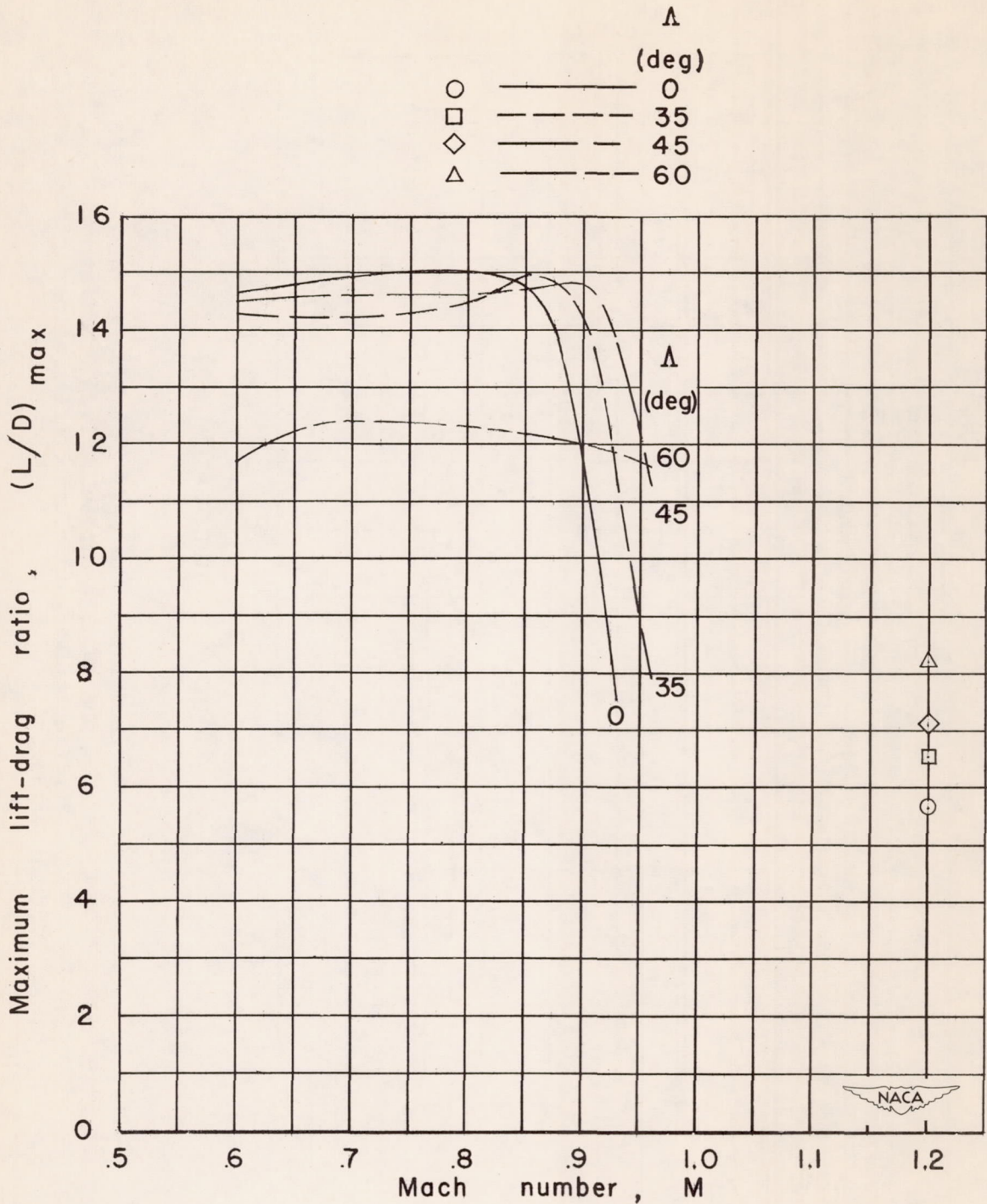
Figure 12.- Variation of maximum lift-drag ratio with Mach number at various angles of sweepback. Drag coefficient corrected for sting interference; wing-fuselage configuration; NACA 65A006 airfoil section, $A = 4$, $\lambda = 0.6$.
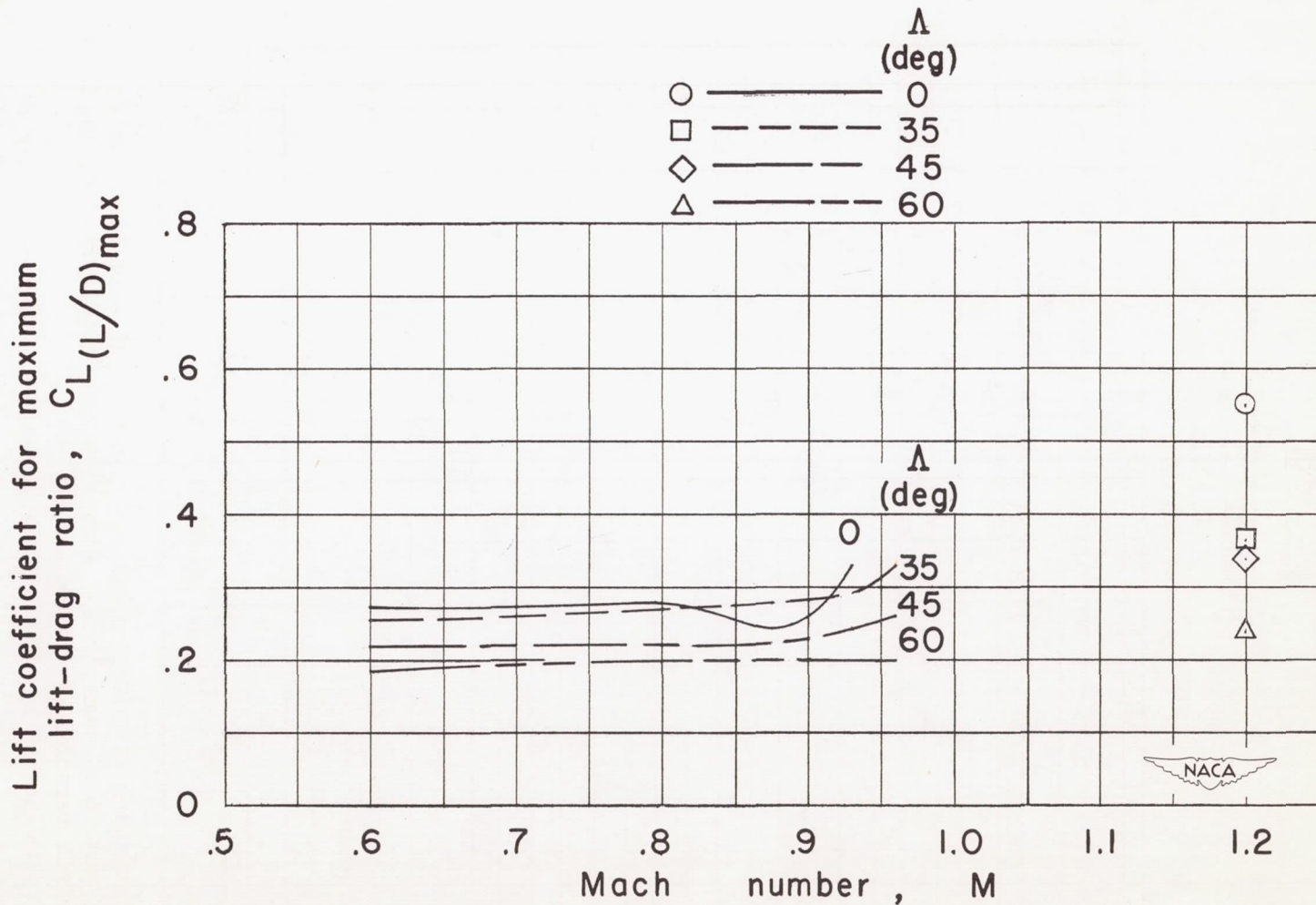
Figure 13.- Variation of lift coefficient for maximum lift-drag ratio with Mach number at various angles of sweepback. Drag coefficient corrected for sting interference; wing-fuselage configuration; NACA 65A006 airfoil section, A = 4, λ = 0.6.
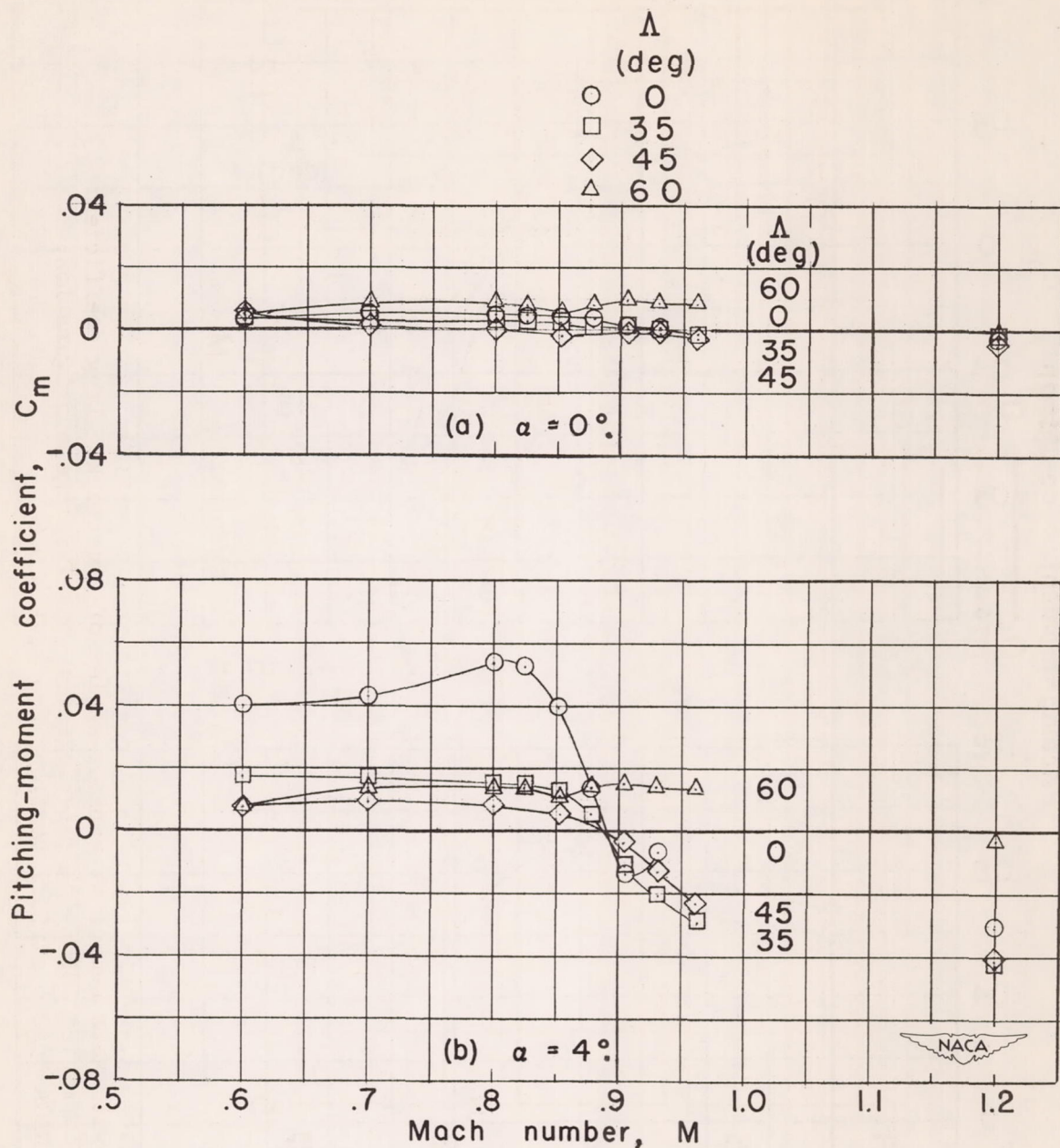
Figure 14.- Variation of pitching-moment coefficient with Mach number
at various angles of sweepback. Wing-fuselage configuration; NACA
65A006 airfoil section, A = 4, λ = 0.6.

Figure 14.- Concluded.

Figure 15.- Variation of pitching-moment coefficient with Mach number
at various angles of sweepback. Wing-fuselage configuration; NACA
65A006 airfoil section, A = 4, λ = 0.6.

Figure 16.- Variation of pitching-moment coefficient with lift
coefficient at various angles of sweepback. Wing-fuselage
configuration; NACA 65A006 airfoil section, A = 4, λ = 0.6.
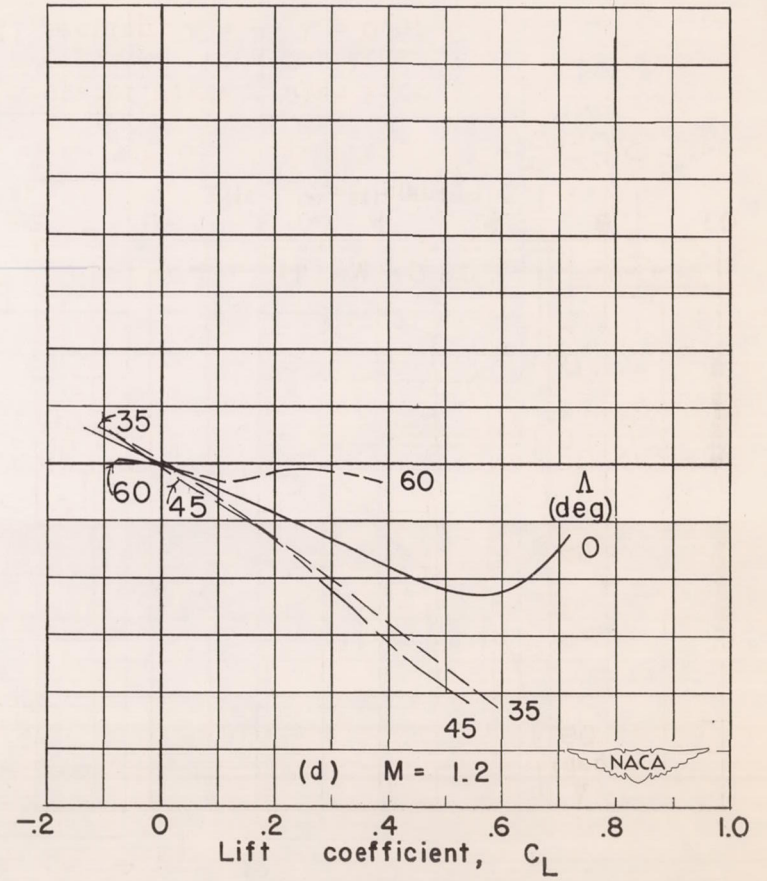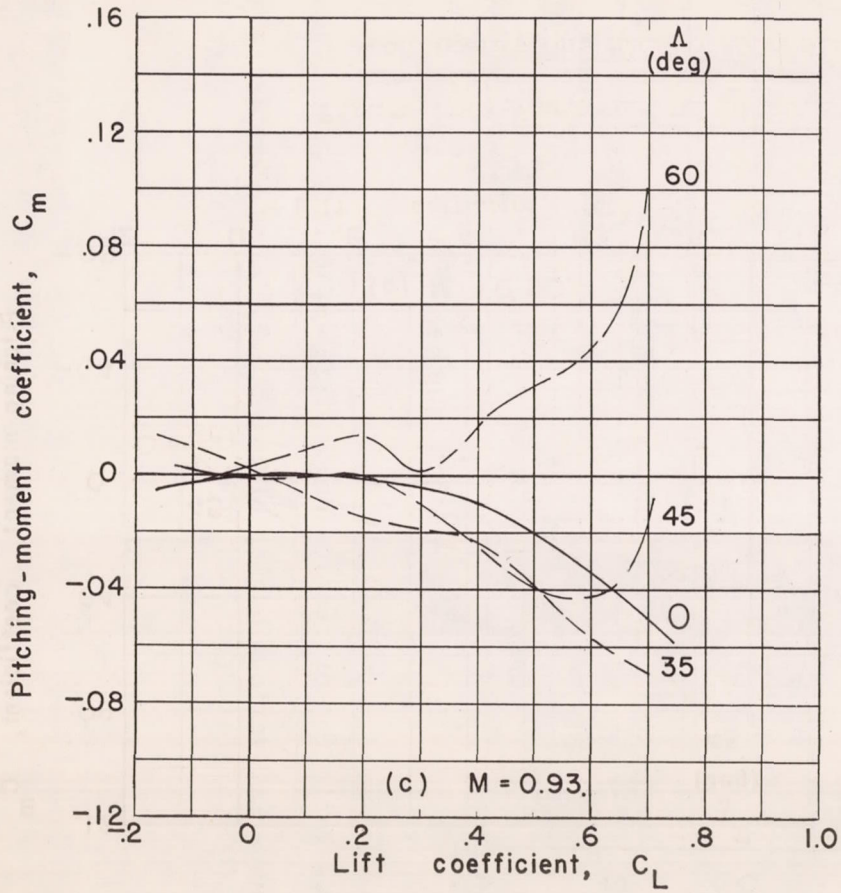
Figure 16.- Concluded.
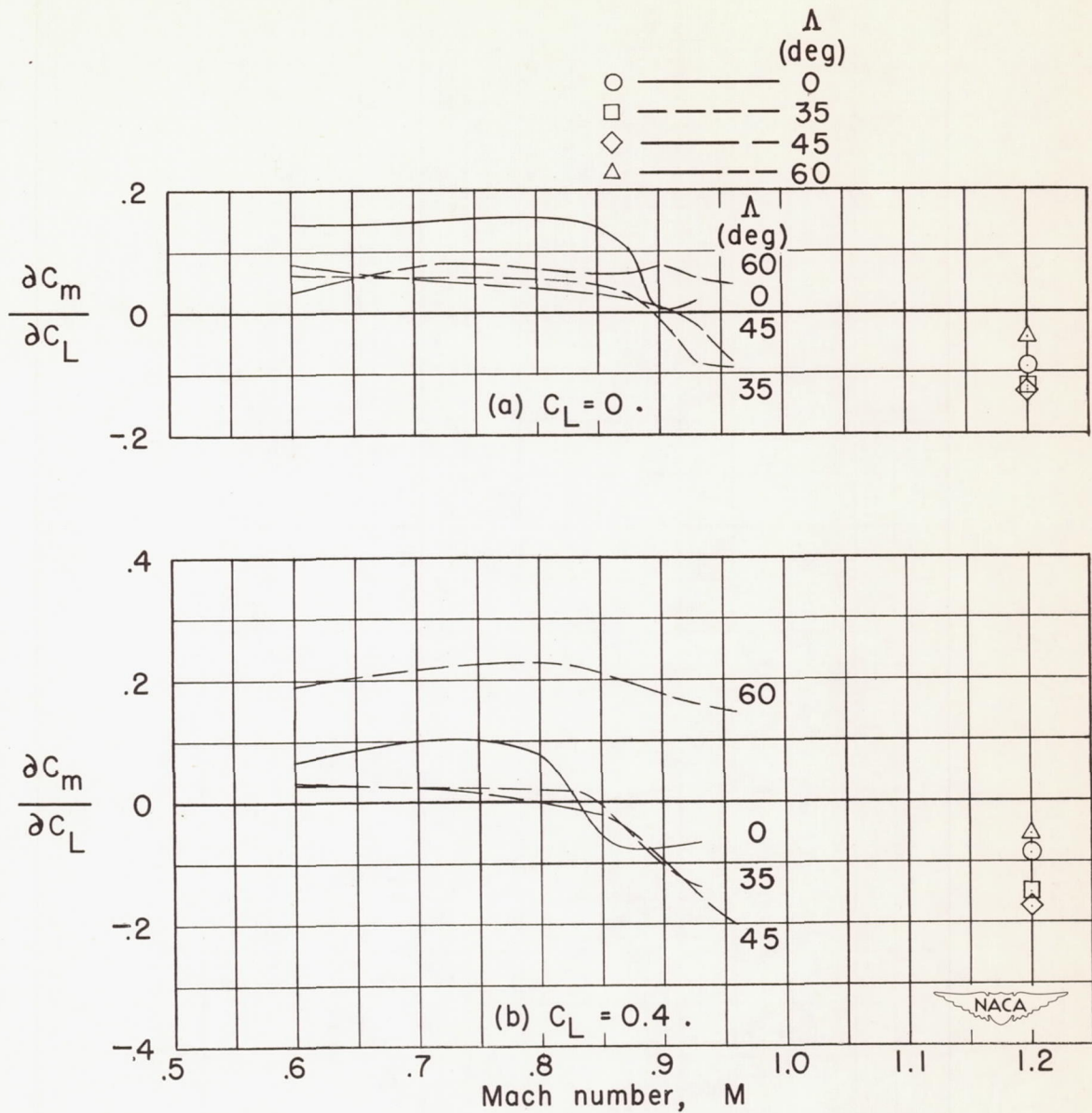
Figure 17.- Variation of static-longitudinal-stability parameter $\dfrac{\partial C_m}{\partial C_L}$ with

Mach number at various angles of sweepback. Wing-fuselage configuration; NACA 65A006 airfoil section, A = 4, λ = 0.6.
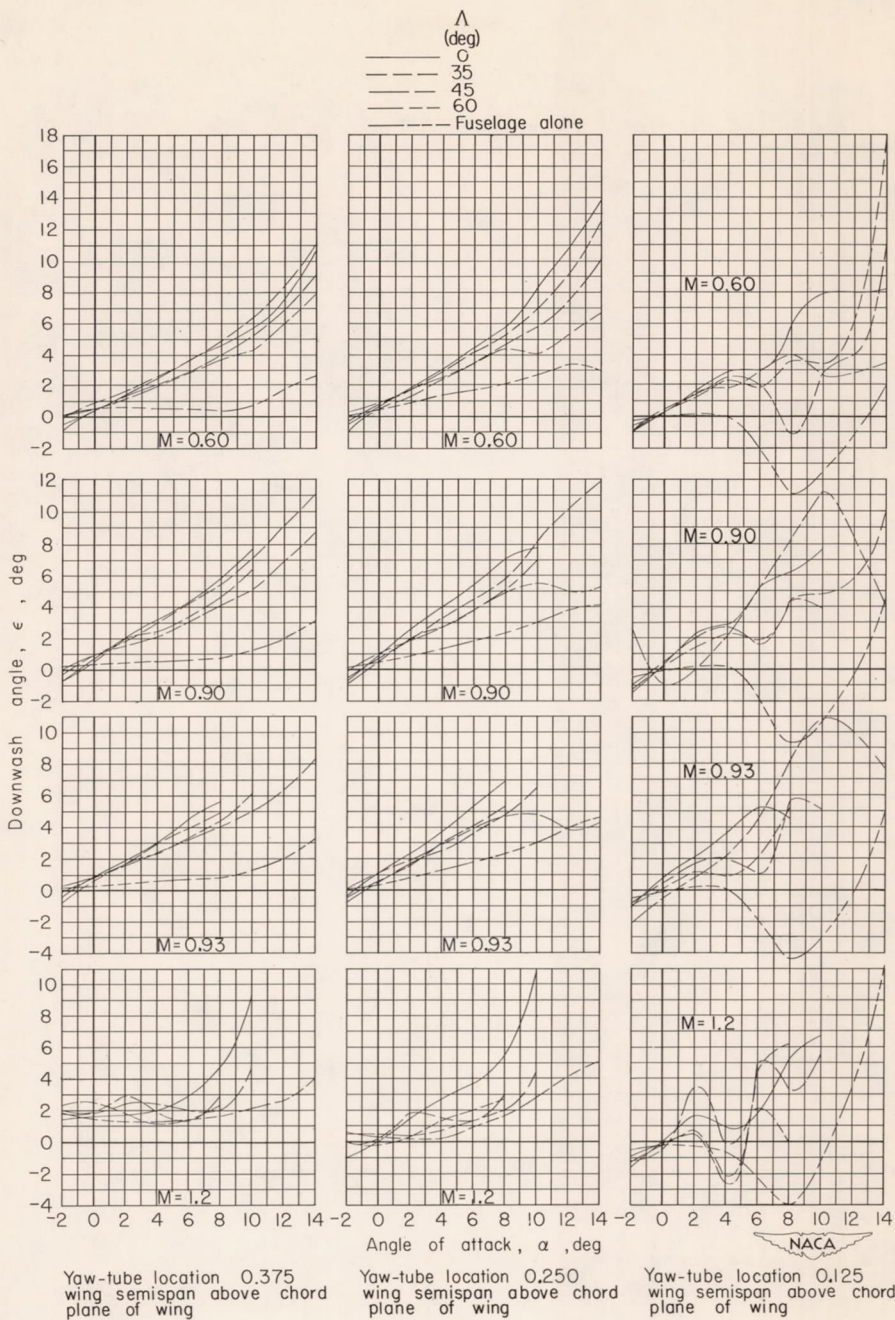
(a) Rake location 0.083 wing semispan from
plane of symmetry of model.
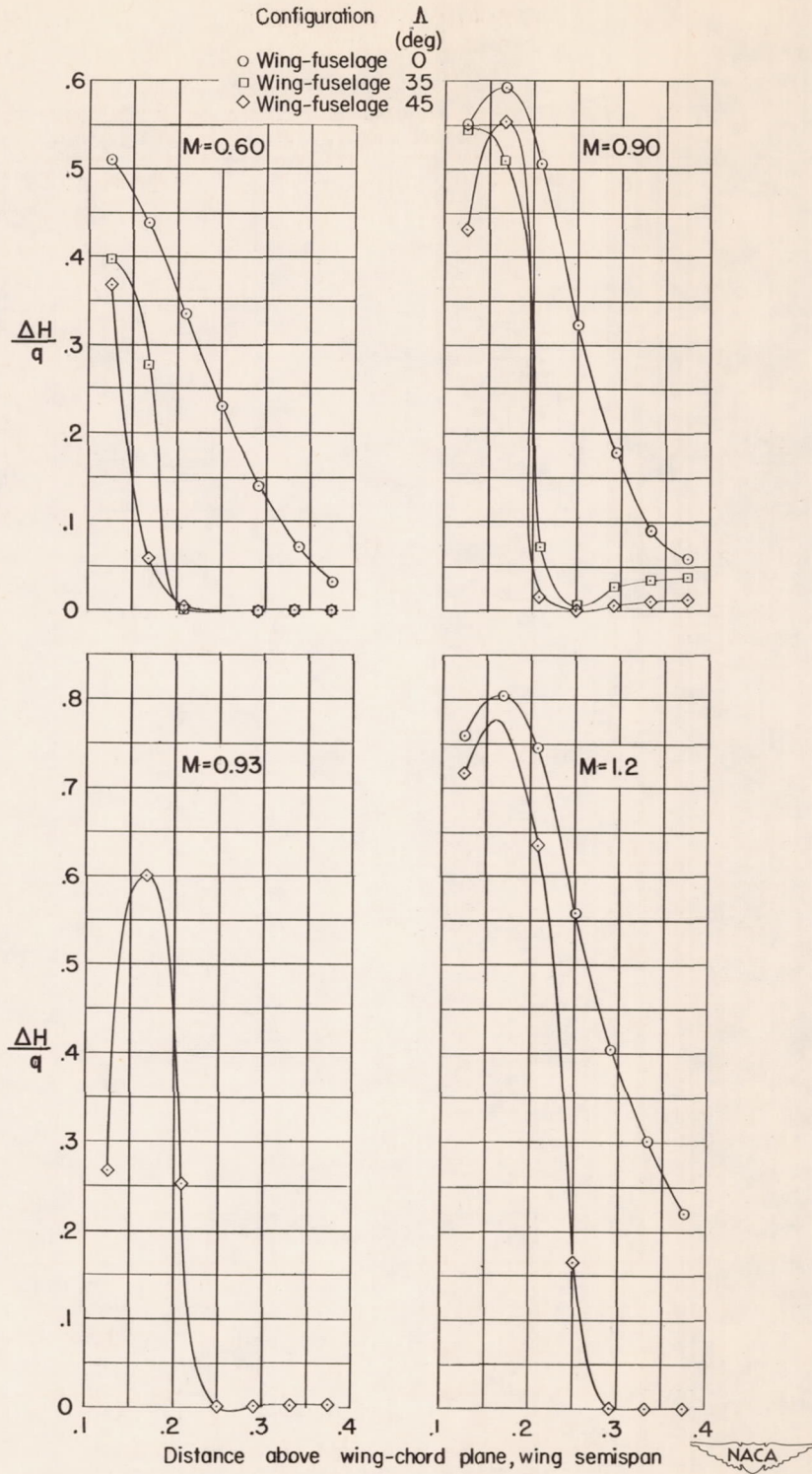
Figure 18.- Point downwash measurements 1.225 wing semispans behind
25-percent point of mean aerodynamic chord of wing (0.25c' point
located at maximum diameter of fuselage). Wing-fuselage configu-
ration and fuselage alone; NACA 65A006 airfoil section, A = 4,
λ = 0.6.
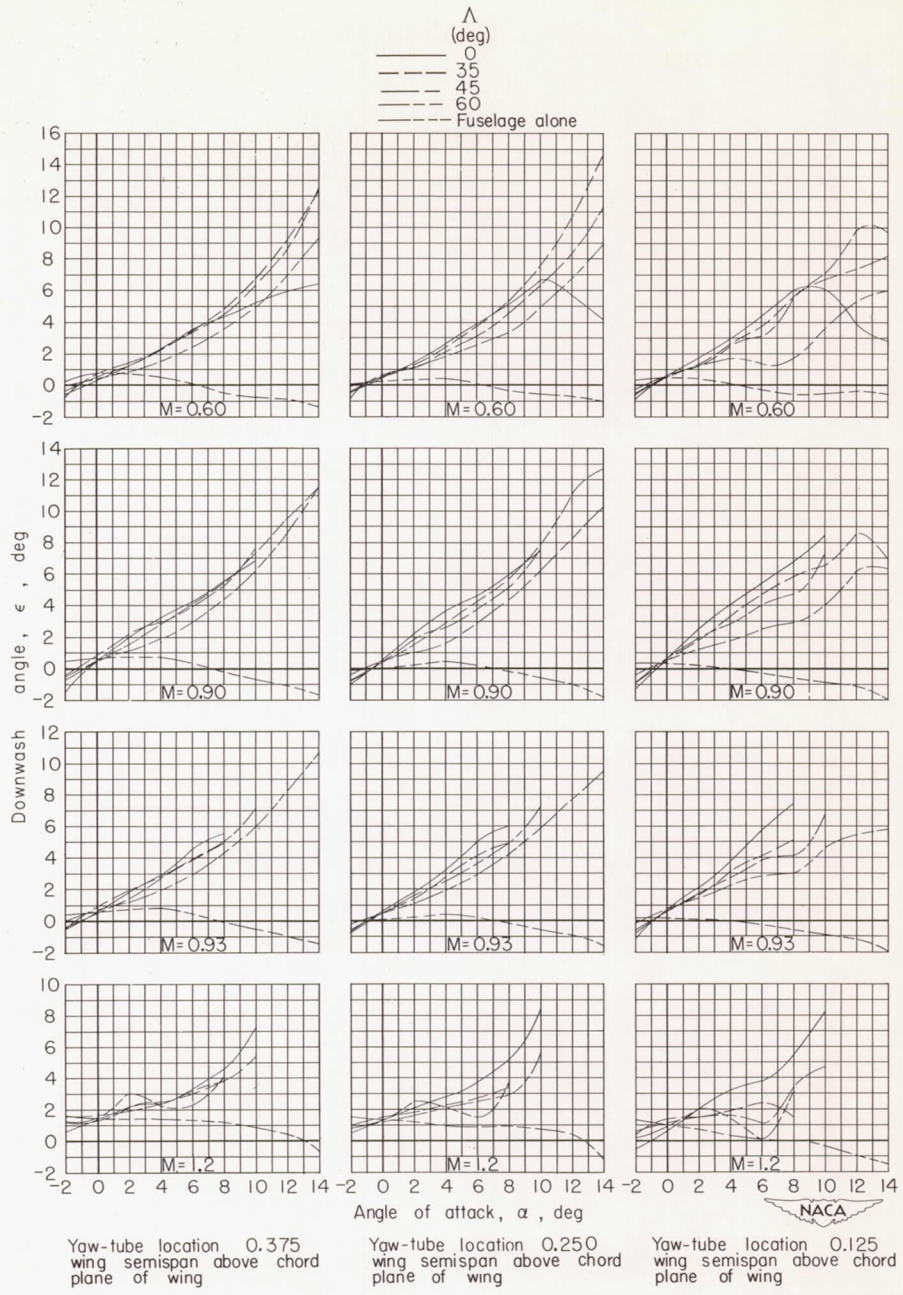
(b) Rake location 0.292 wing semispan from
plane of symmetry of model.

Figure 18.- Concluded.
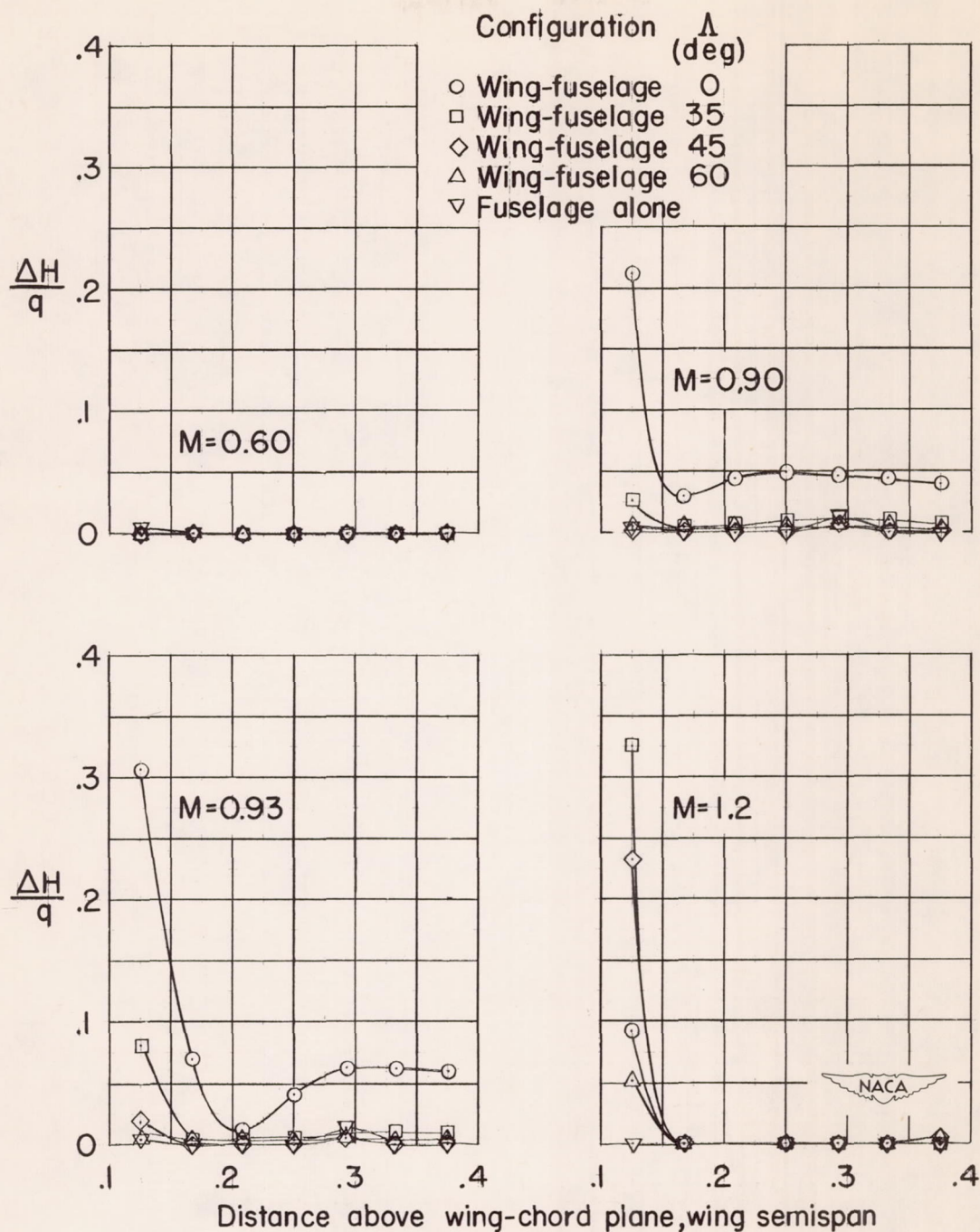
(a) α = 4°.

Figure 19.- Wake measurements 1.225 wing semispans behind 25-percent point
    of mean aerodynamic chord of wing (0.25c' point located at maximum
    diameter of fuselage) and 0.083 wing semispan from plane of symmetry of
    model. Wing-fuselage configuration and fuselage alone; NACA 65A006 air-
    foil section, A = 4, λ = 0.6.
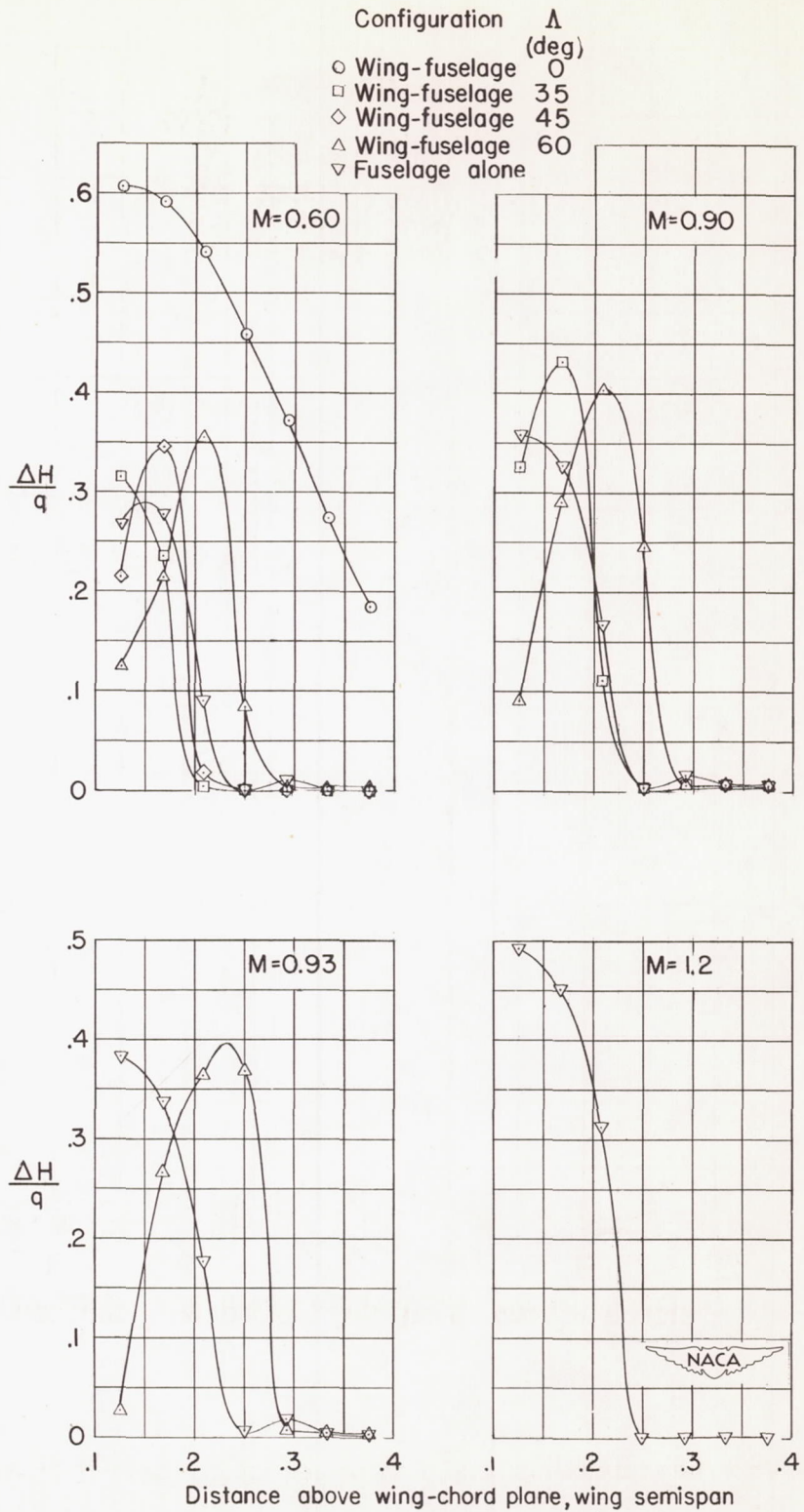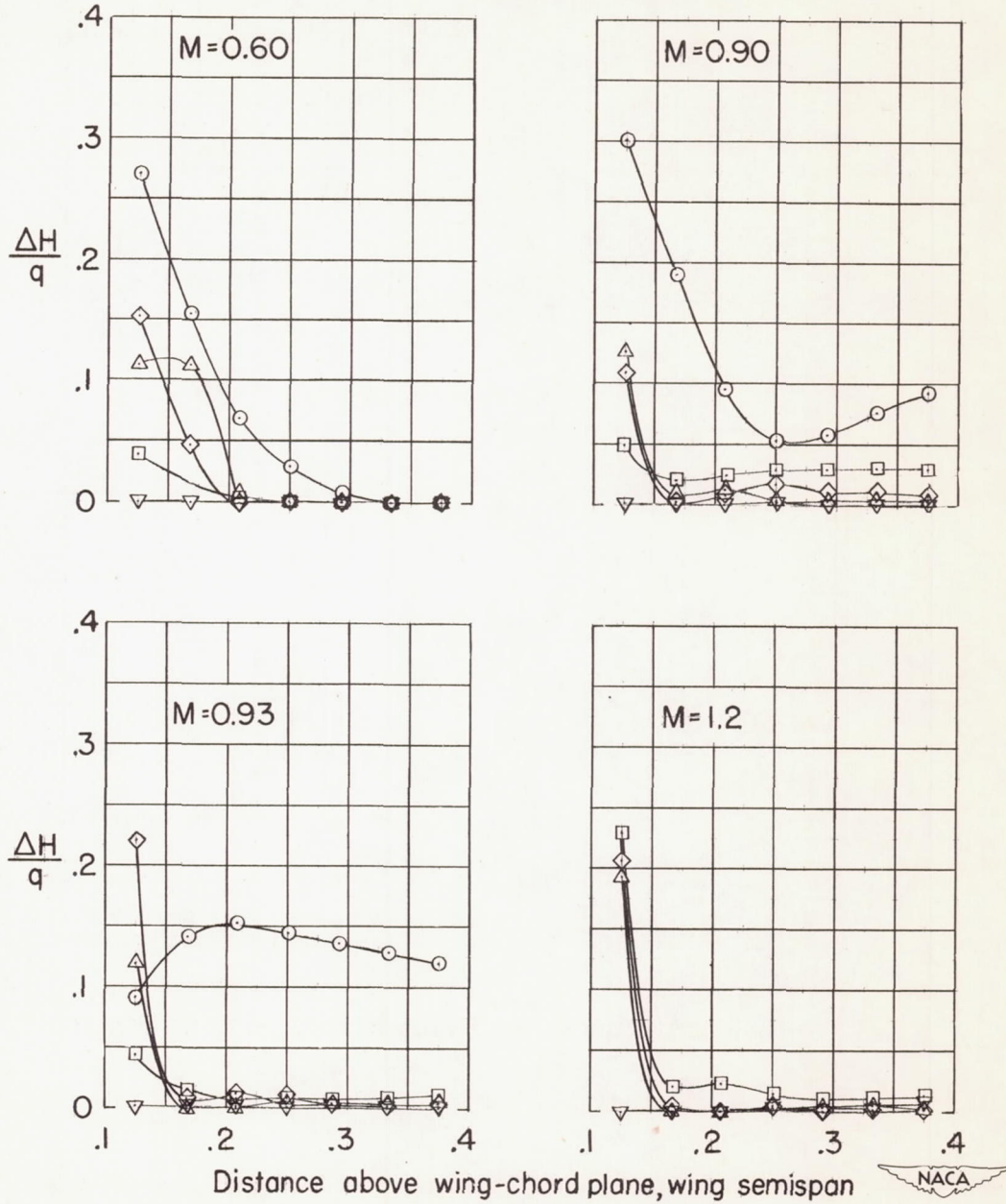
Configuration Λ
(deg)
○ Wing-fuselage 0
□ Wing-fuselage 35
◇ Wing-fuselage 45
△ Wing-fuselage 60
▽ Fuselage alone

Distance above wing-chord plane, wing semispan

(b) $\alpha = 8^{o}$.
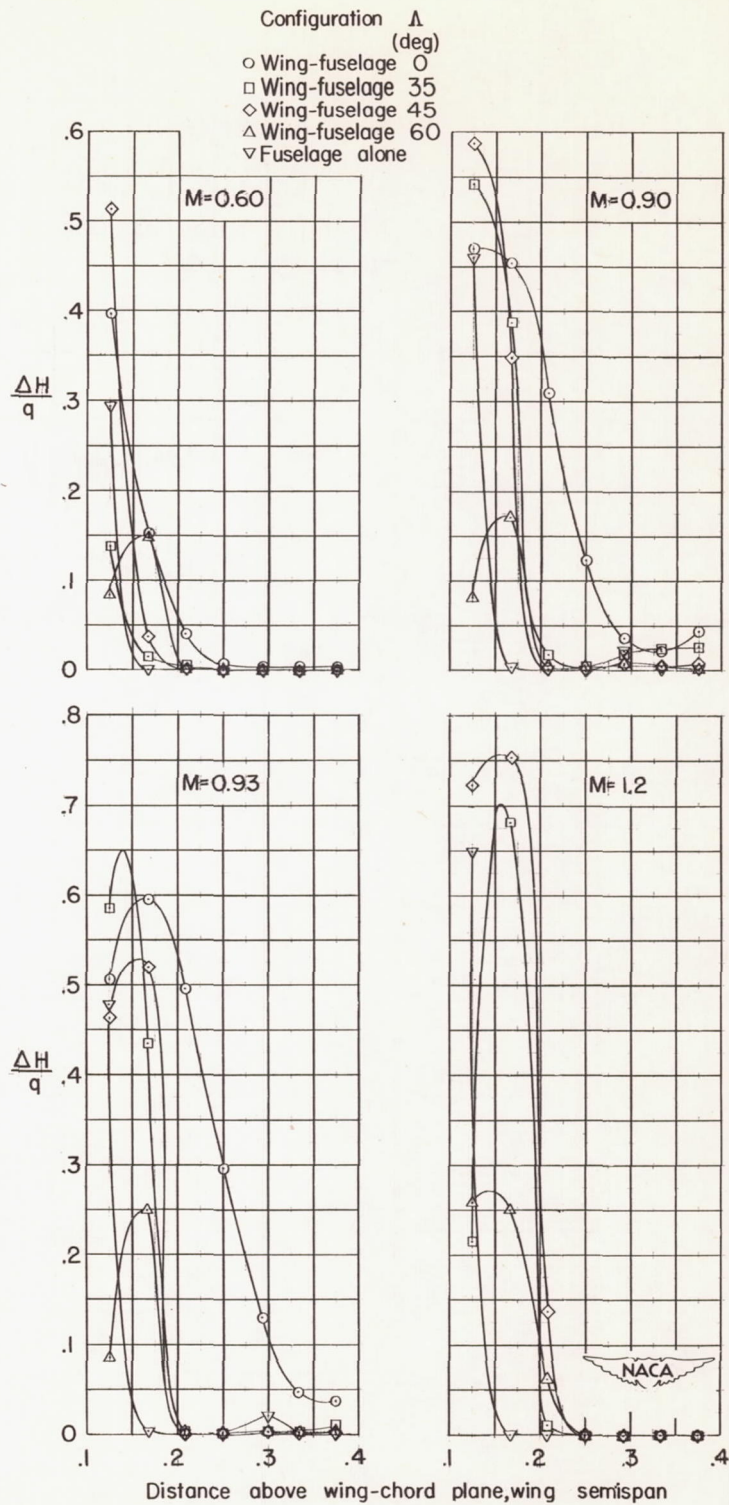
Figure 19.- Continued.

(c) $\alpha = 10^{\circ}$.

Figure 19.- Continued.

Configuration   Λ
                 (deg)
○ Wing-fuselage   0
□ Wing-fuselage   35
◇ Wing-fuselage   45
△ Wing-fuselage   60
▽ Fuselage alone

M=0.60

M=0.90

$\frac{\Delta H}{q}$

M=0.93

M=1.2

NACA

$\frac{\Delta H}{q}$

Distance above wing-chord plane, wing semispan

(d)   α = 12°.

Figure 19.- Concluded.
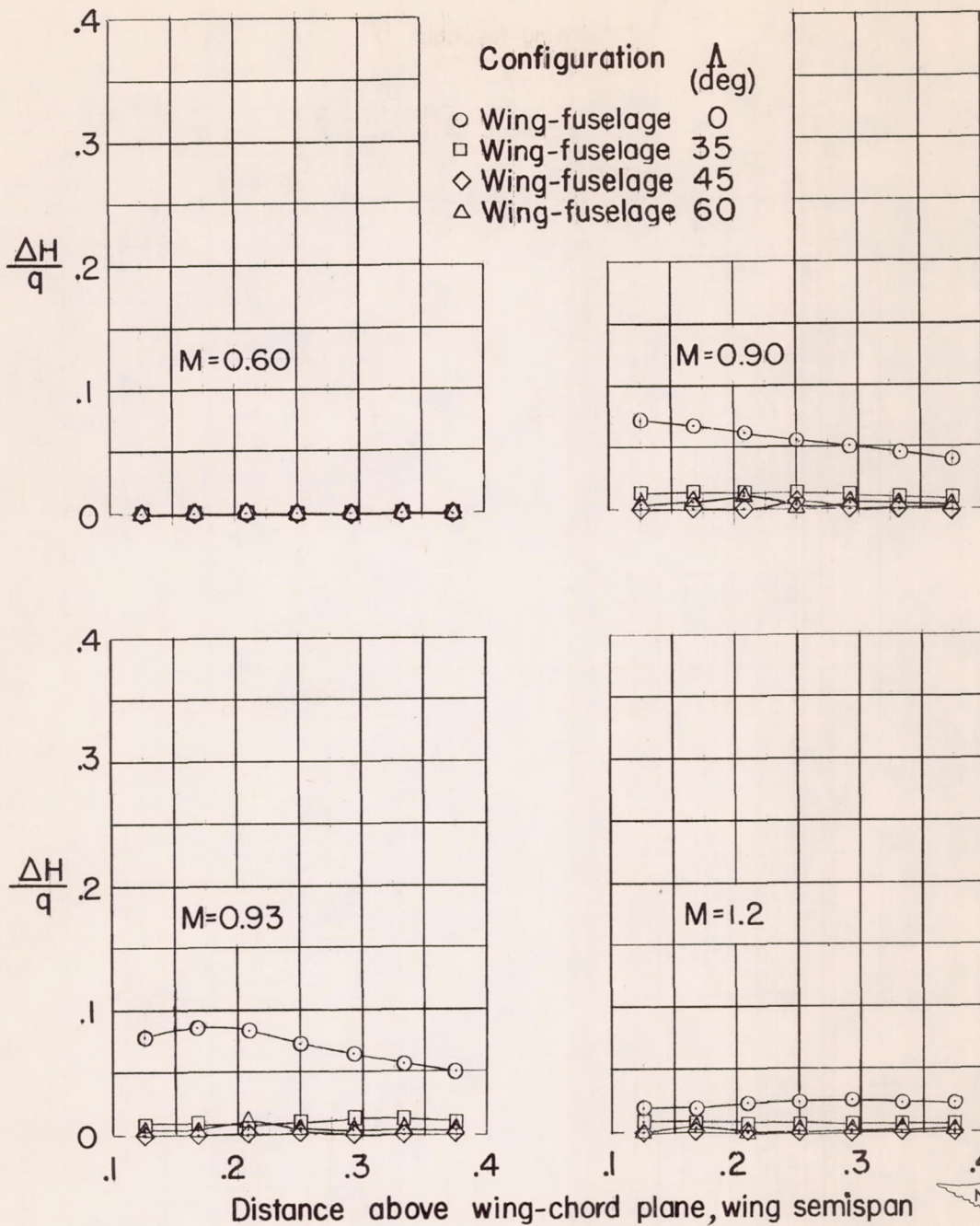
(a) α = 4°.

Figure 20.- Wake measurements 1.225 wing semispans behind 25-percent point
    of mean aerodynamic chord of wing (0.25c' point located at maximum
    diameter of fuselage) and 0.292 wing semispan from plane of symmetry of
    model. Wing-fuselage configuration and fuselage alone; NACA 65A006 air-
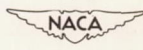   foil section, A = 4, λ = 0.6.

Configuration Λ
(deg)
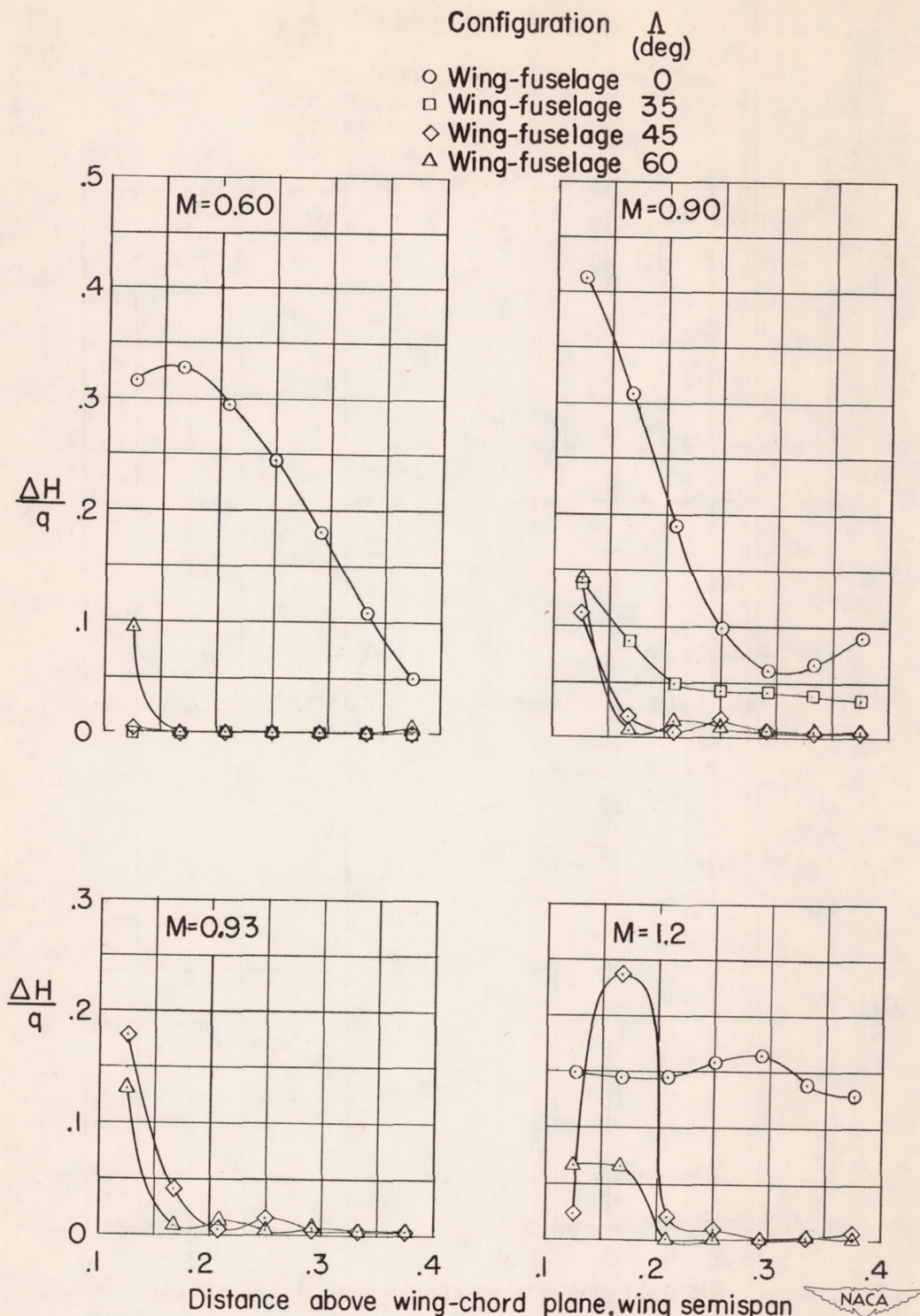○ Wing-fuselage   0
□ Wing-fuselage   35
◇ Wing-fuselage   45
△ Wing-fuselage   60
▽ Fuselage alone

(b) $\alpha = 8^\circ$.

Figure 20.- Continued.

(c) α = 10°.

Figure 20.- Continued.

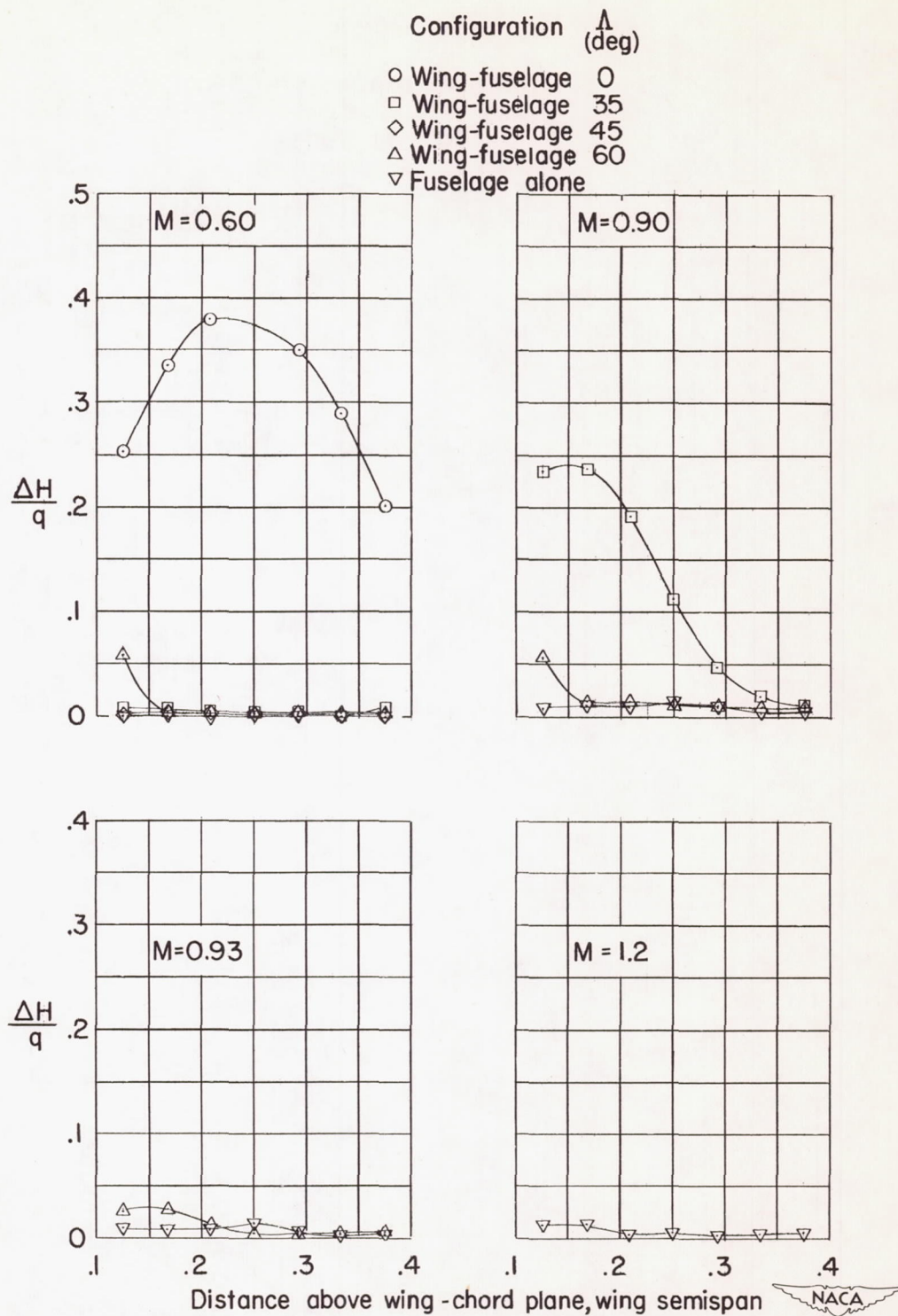Configuration Λ (deg)

○ Wing-fuselage 0
□ Wing-fuselage 35
◇ Wing-fuselage 45
△ Wing-fuselage 60
▽ Fuselage alone

(d) $\alpha = 12^{o}$.

Figure 20.- Concluded.

Λ
(deg)
○ 0
□ 35
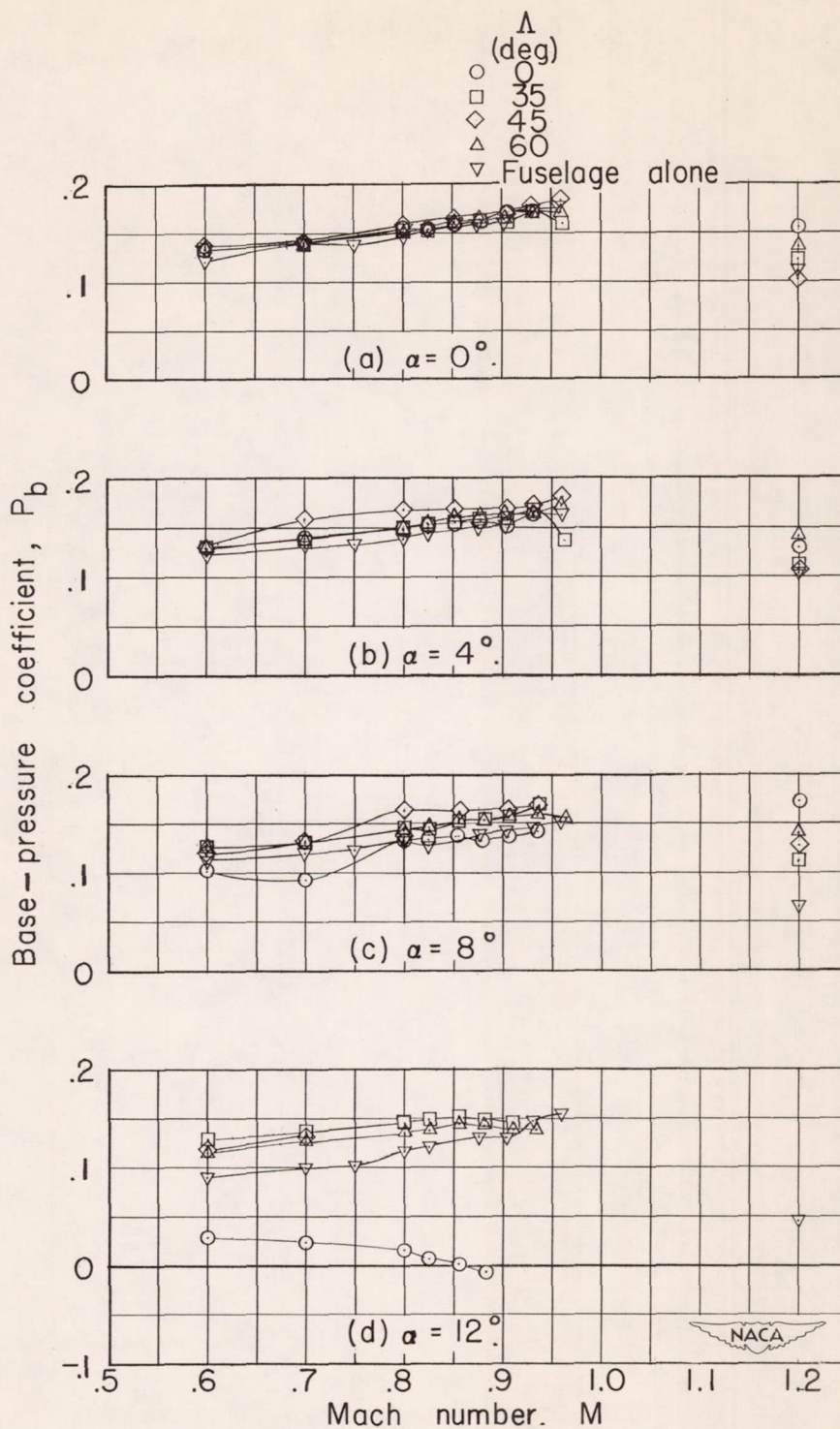◇ 45
△ 60
▽ Fuselage alone

Figure 21.- Variation of base-pressure coefficient with Mach number at various angles of sweepback. Wing-fuselage configuration and fuselage alone; NACA 65A006 airfoil section, A = 4, λ = 0.6.